WINTER AND SUMMER SIMULATIONS WITH THE ECMWF MODEL

M.Tiedtke

ECMWF

ABSTRACT

Winter and summer simulations have been carried out with the ECMWF operational medium range forecast model. It is a 15-level grid point model of resolution N48 and incorporates the parameterization of radiative processes, large-scale condensation, cumulus convection and turbulent exchange of heat, moisture and momentum. The integrations start from real data of 21 January and 11 June respectively, and the simulated flow of the 20 to 50 day period is studied and compared with observations. The main results are: The global distribution of the mean flow appears realistic except for the following noticeable differences to observations:

The Icelandic Low is displaced eastward.

The Aleutian Low is overdeveloped

The Atlantic High is displaced northward and the subtropical tradewinds over the Atlantic are therefore too weak.

The upper tropospheric easterly flow is more intense between the Pacific and Africa.

The Walker circulation is more intense over the Pacific in the summer simulation.

The Hadley circulation is weaker in all branches except over Indonesia/Western Pacific.

A serious problem is that the troposphere is systematically colder and the stratosphere is much too cold at middle and high latitudes. The subtropical jets are realistically closed off and clearly separated from the polar night jet but they are more intense and shifted upward and poleward. The westerly flow is increased at mid-latitudes and decreased at high latitudes.

The evaluation of the energy cycle shows that:

The eddy kinetic energy is smaller than observed.

The energy conversions, particularly the baroclinic conversions are nevertheless, far more intense.

Too much eddy available potential energy seems to be generated by diabatic heating.

It is also found that despite the weaker transient edddies, the meridional transport of momentum and sensible heat is larger than observed. The simulation of the long standing waves at higher latitudes is poor, which largely effects the meridional momentum transports. The diabatic forcing fields are realistic. The distribution of precipitation and surface fluxes of sensible and latent heat agree well with observations. The surface stress is, however, far too intense along the cyclone tracks in both hemispheres. The net diabatic heating appears too strong over Indonesia and the western Pacific, and too weak over the Atlantic.

Finally, a sensitivity experiment is described where the Kuo convection scheme is replaced by the Arakawa-Schubert scheme. A winter simulation experiment was carried out with this scheme and the simulated mean flow was compared with that of the standard simulation experiment. Large differences in the mean tropical and extratropical flow are found which are caused by differencces in the diabatic heating in the tropics. Detailed diagnostics of the diabtic heating indicate that the large differences obtained for the convective heating are mainly due to differences in the net radiative flux over land which result from differences in the cloud cover for the radiation calculation. It is concluded, that the parameterization of clouds for the radiation calculation must be improved in the EC-model before convection schemes can really be tested in global integrations.

1. INTRODUCTION

Medium range forecasts up to 10 days have been carried out at ECMWF since August 1979. Subjective as well as objective verifications of the operational forecasts show that they are generally useful up to 4 to 5 days but have a number of systematic errors which grow rapidly in time and can therefore significantly affect the forecast quality beyond day 5. The consistency of these errors suggests that they are independent of the initial flow but indicates a trend towards a climate in the forecast which differs from that of the atmosphere. It was therefore decided to carry out extended integrations up to 50 days and to study the simulated flow and its deviations from the mean observed flow. These integrations indeed proved that the model's climate deviates significantly from that of the atmosphere and it became evident that the characteristic errors are very similar to those observed in our medium range forecasts. This paper presents the analysis of winter and summer circulations simulated by the operational forecast model of ECMWF. Emphasis is put on the graphical presentation of the results and the discussions are restricted to the main points as far as possible. The results are presented in the following order:

1. Global distribution of the mean flow
2. The globally averaged state and the energy cycle
3. The zonally averaged flow and its forcing
4. The geographical distribution of the diabatic forcing

In the last section we describe a winter simulation experiment to study the sensitivity of the simulated mean flow to the parameterization of convection.

2. MODEL DESCRIPTION

The integrations were performed with the operational ECMWF grid point model, as described by Burridge and Haseler (1977) and by Tiedtke et al (1979). Its basic features are summarized opposite:

3. INITIAL CONDITIONS AND BOUNDARY CONDITIONS

Both integrations started from real data of the FGGE observing period, i.e. from 21 January 1979 and from 11 June 1979.

The topography (Fig.1) used in both runs is the revised version which has been introduced into the ECMWF operational forecast model in December 1981. This topography is based on the US Navy 10' orography adapted to our N48 lat-long grid and subjected to a grid point filter for smoother fields. The sea surface temperatures have been derived from the Rand 1° x 1° climatology (Crutcher and Jenne, 1970). Seasonal changes of the surface albedo due to changes in the vegetation are presently not considered in the EC model. The geographical distribution of the surface albedo is therefore identical in both runs except for the change in snow and ice cover. Values over sea were set to 0.07, over sea ice to 0.55 and land values range from 0.07 to 0.80. The value over snow was set to 0.80.

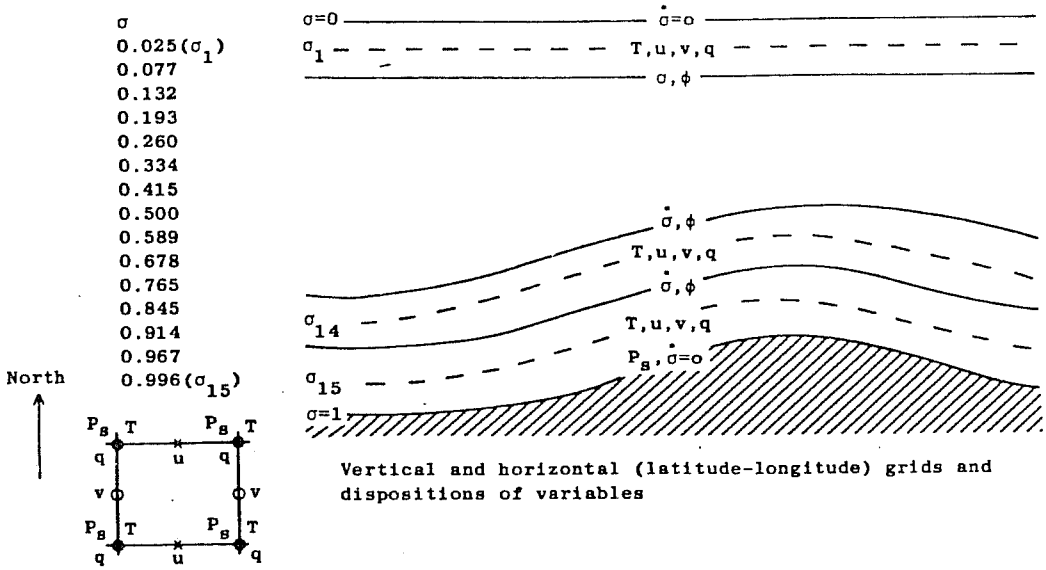

Vertical and horizontal (latitude-longitude) grids and dispositions of variables

Independent variables:	ψ, λ, σ, t
Prognostic variables:	p_s, T, u, v, q
Diagnostic variables:	ϕ , $\dot{\sigma} = \frac{d\sigma}{dt}$
Grid:	Arakawa C-grid, N48, uniform in λ, ϕ ($\Delta\lambda = \Delta\phi = 1.875^{o}$) 15 levels, non-uniform vertical spacing (see above).
Finite difference scheme:	Second order accuracy.
Time integration:	Leapfrog, semi-implicit (Δt = 15) Weak time filter (ν = 0.05)
Turbulent processes:	Stability dependent vertical diffusion of T, u, v, q, within the surface layer after Monin-Obukov.
Cumulus convection:	Kuo (1974)
Radiation:	1. Use of model generated clouds. 2. No daily variation of solar radiation.
Horizontal diffusion:	Linear 4th order
Land surface pressures:	Prognoses of soil temperature, soil water and snow amount.

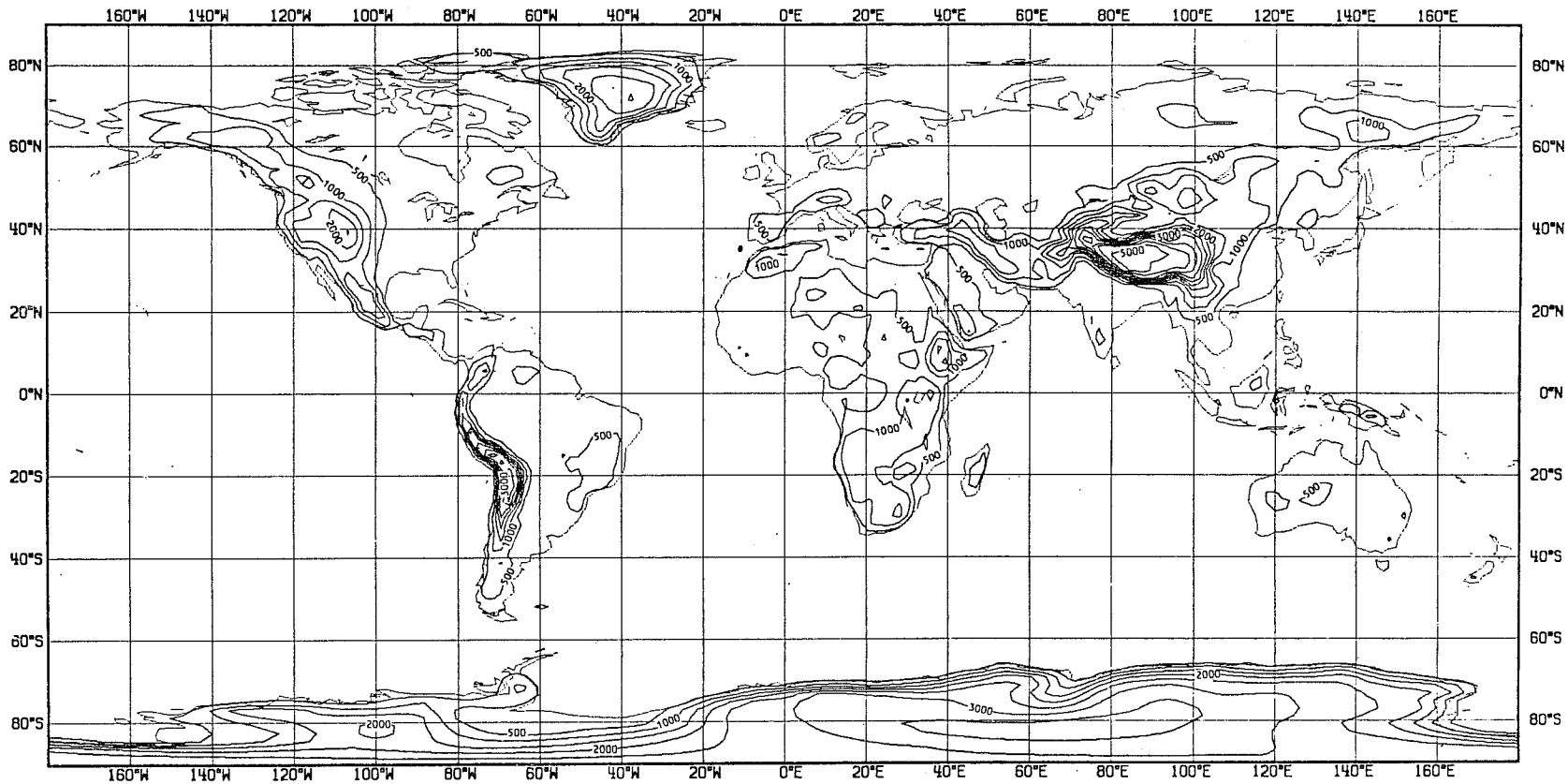

Fig. 1 Orography used in the winter and summer simulations. (Contour interval is 500 m).

4. THE SIMULATED FLOW

4.1 Global distribution of the mean flow

(a) Geopotential height fields

For completeness, global as well as Northern Hemispheric maps are presented. The simulated height fields are compared with the monthly mean height fields for February and July 1979 respectively, and also with the climate height fields for February and July. The simulated global height fields (Figs.2,3) contain the major circulation features which are observed in summer and winter respectively. The simulated 1000 mb height field, for example, shows the tropical continental lows, the subtropical highs, the strong westerly flow in the Southern Hemisphere, the Icelandic low, the Aleutian lows and the Siberian High. There are, however, large differences in location and intensity of the pressure systems. The most striking errors are the eastward displacement of the Icelandic low and the overdevelopment of the Aleutian low in the winter simulation. A consequence of these errors is a westerly flow over North America, Europe and Asia, instead of the observed north-easterly and south-westerly flow, respectively. The mean height field appears to be better simulated in summer, but we find similar errors as in winter, i.e. there is again an eastward displacement of the Icelandic low at 1000 mb and of the 500 mb Atlanic trough, as well as an intensification of the westerly flow over the North Pacific at the surface.

The errors in the height fields are essentially of a barotropic nature as they are very similar at 500 mb and 1000 mb which is best seen from the maps showing the differences to observations (not displayed here).

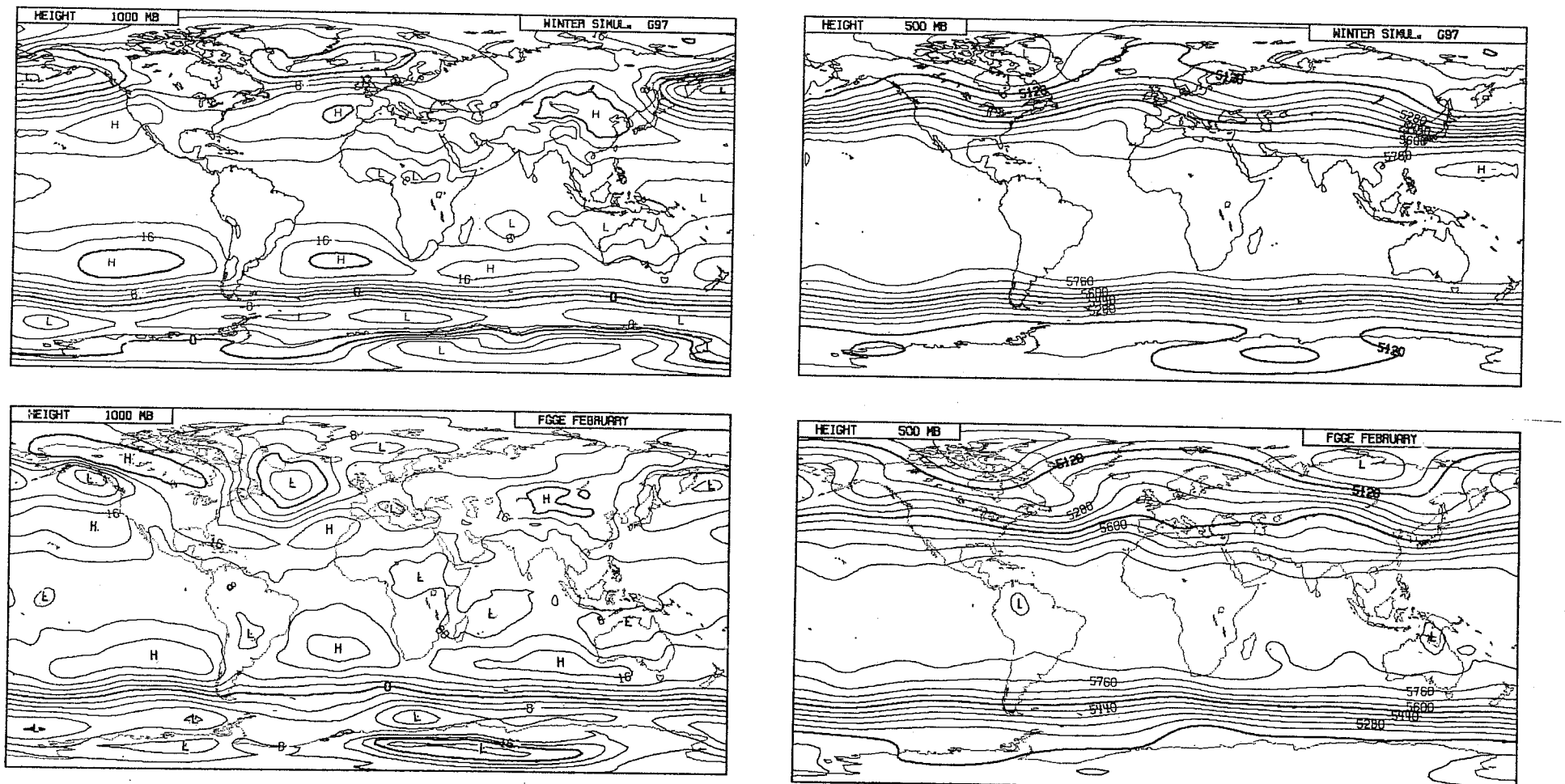

Fig. 2 Geopotential heights for winter simulation experiment G97 (30 day mean) and observed heights in February 1979.

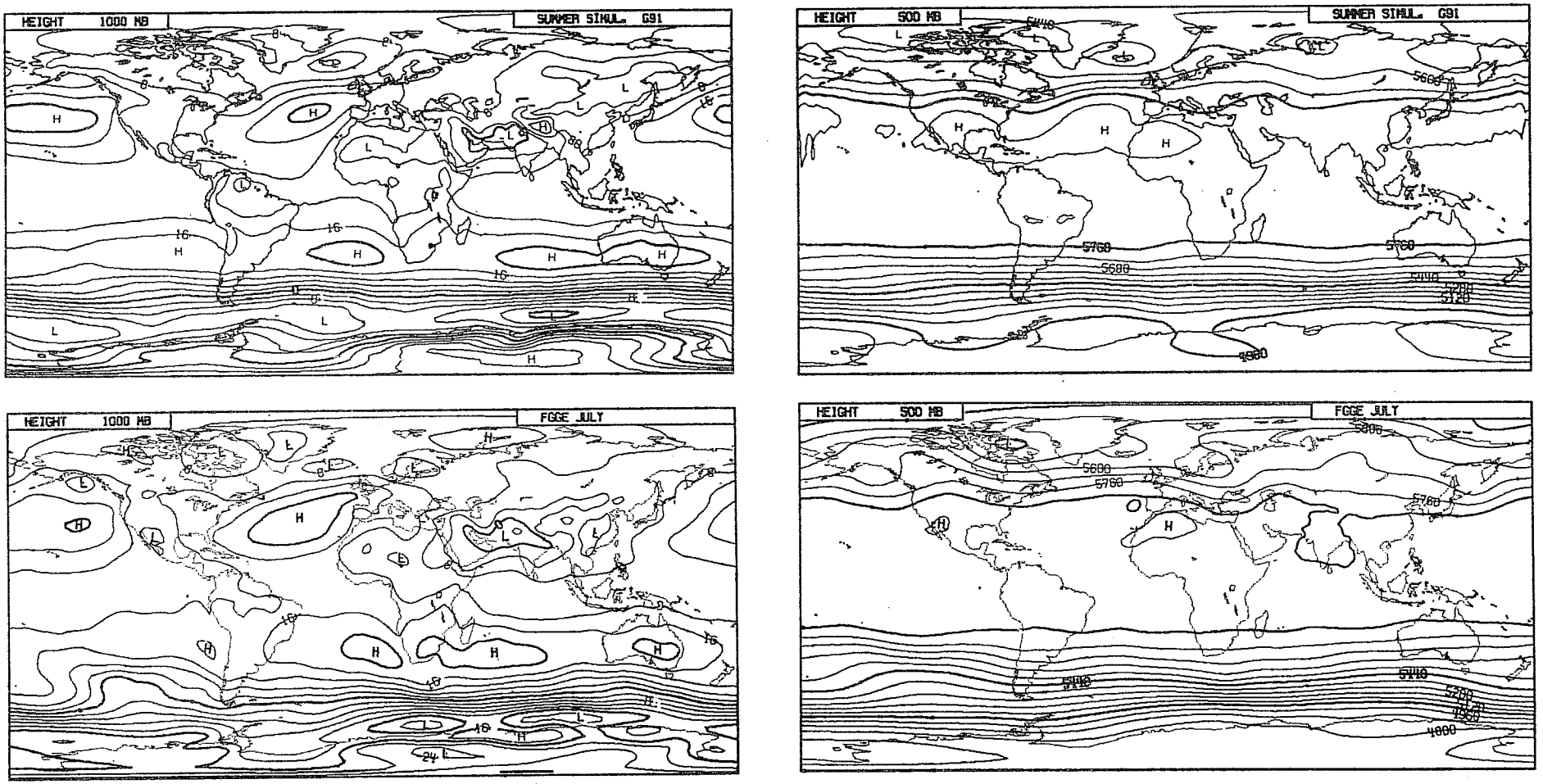

Fig. 3 As Fig. 2 but for summer simulation experiment G91 and for July 1979.

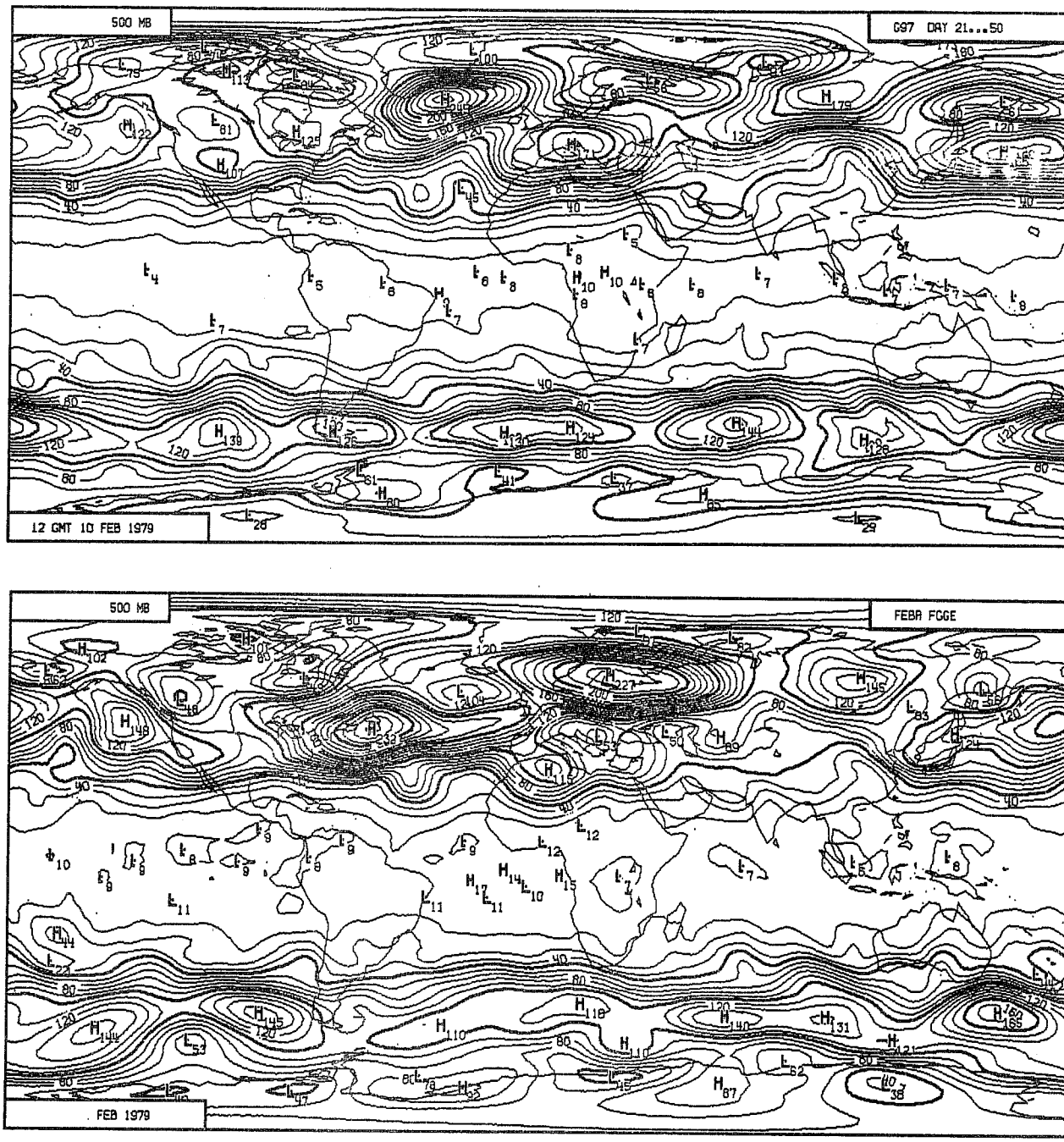

Fig. 4 Variance of the 500 mb height field due to transient waves.

Top: Winter simulation, day 20-50.
Bottom: February 1979 (ECMWF analysis).

(b) The variance of the height fields due to transient eddies

Fig.4 shows the rms deviations of the 500 mb and 1000 mb height fields for the winter simulation and for the atmosphere during February 1979. These fields represent the local variability due to fluctuations of all inherent frequencies. The observed fields shows the largest variances over the oceans along the cyclone tracks which indicate that the medium long baroclinic eddies account for most of the variances. Both simulations produce variances of similar intensities than observed, (Fig.4). The comparable level of variance in the simulation and the observation is significant in view of the energy cycle, discussed later where it is seen that despite realistic variances the baroclinic energy conversions are much more intense in the simulation than observed.

(c) Streamfunction

The streamfunction (not displayed here) reflects the same characteristic features in the extratropics as the geopotential height fields. The simulated flow in the tropics and subtropics is in broad agreement with observation, but differs from the observed flow in some areas. Since the fields are not presented, we mention here only:

1. An increased upper tropospheric easterly flow extending from the Pacific over Indonesia to Africa. This error is larger and even more widespread in the summer simulation.

2. Weaker tradewinds over the northern Atlantic. This deficiency is connected to the northward displacement of the Atlantic high pressure system. The weakening of the tradewinds implies weaker surface fluxes of latent heat and a weaker surface stress over the Atlantic (see below).

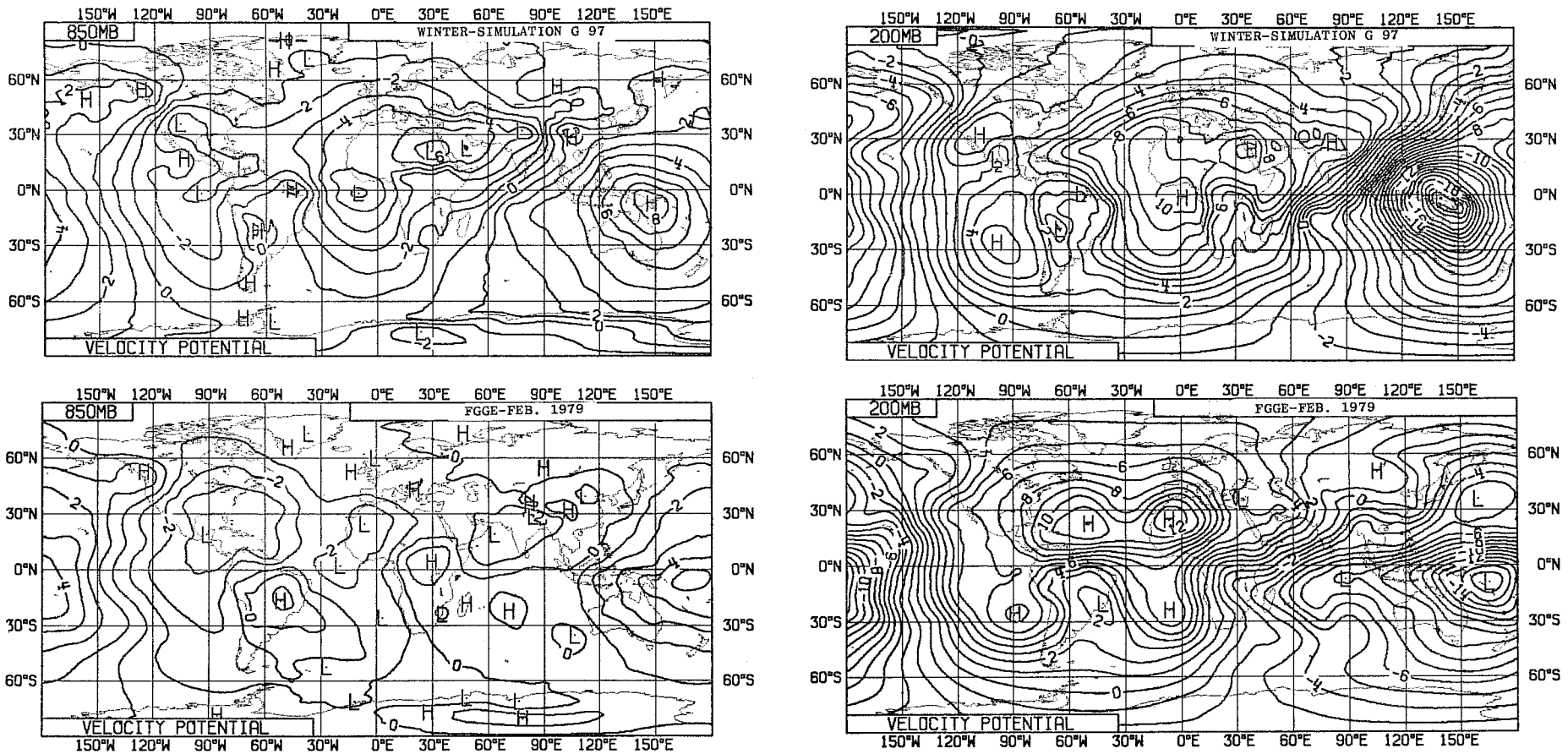

Fig. 5 Winter simulated (top) and observed (bottom) velocity potential at 850 mb and 200 mb.

(d) Velocity potential

The simulated divergent flow as displayed in the velocity potential (Figs.5,6) is again verified against the analysed mean flow of February and July 1979, respectively. It should be mentioned here that this comparison may not be completely conclusive, as the divergent flow is (i) difficult to analyze and (ii) it is presently not known how much the monthly mean divergent flow changes interannually. Despite these uncertainties, the comparison leads to the following conclusions:

The very large-scale distribution of the divergent flow is fairly realistic in both simulations, showing the two main centres of rising and sinking air over the Western Pacific and Atlantic respectively. The divergent flow, however, appears much too intense over the Pacific in the winter simulation. This overintensification is probably related to an excessive diabatic heating in this area (see below).

The medium scale flow is considerably weaker in the simulation and deviates from the observed flow.

In the winter simulation the southerly upper air flow over the north of South America, over the Atlantic and over Africa is largely underestimated, whereas the northern flow over the Indian Ocean and Indonesia is replaced by an excessive north-easterly flow.

The summer simulation fails to reproduce the cross-equatorial flow over the eastern Pacific. Instead, the Walker circulation is much more intense and larger in scale, which is apparent at 850 mb as well as at 200 mb. Over the Atlantic and central Africa we find similar deficiencies, most notable at 200 mb.

Despite these deficiencies the zonally averaged meridional mass fluxes appear realistic in both simulations.

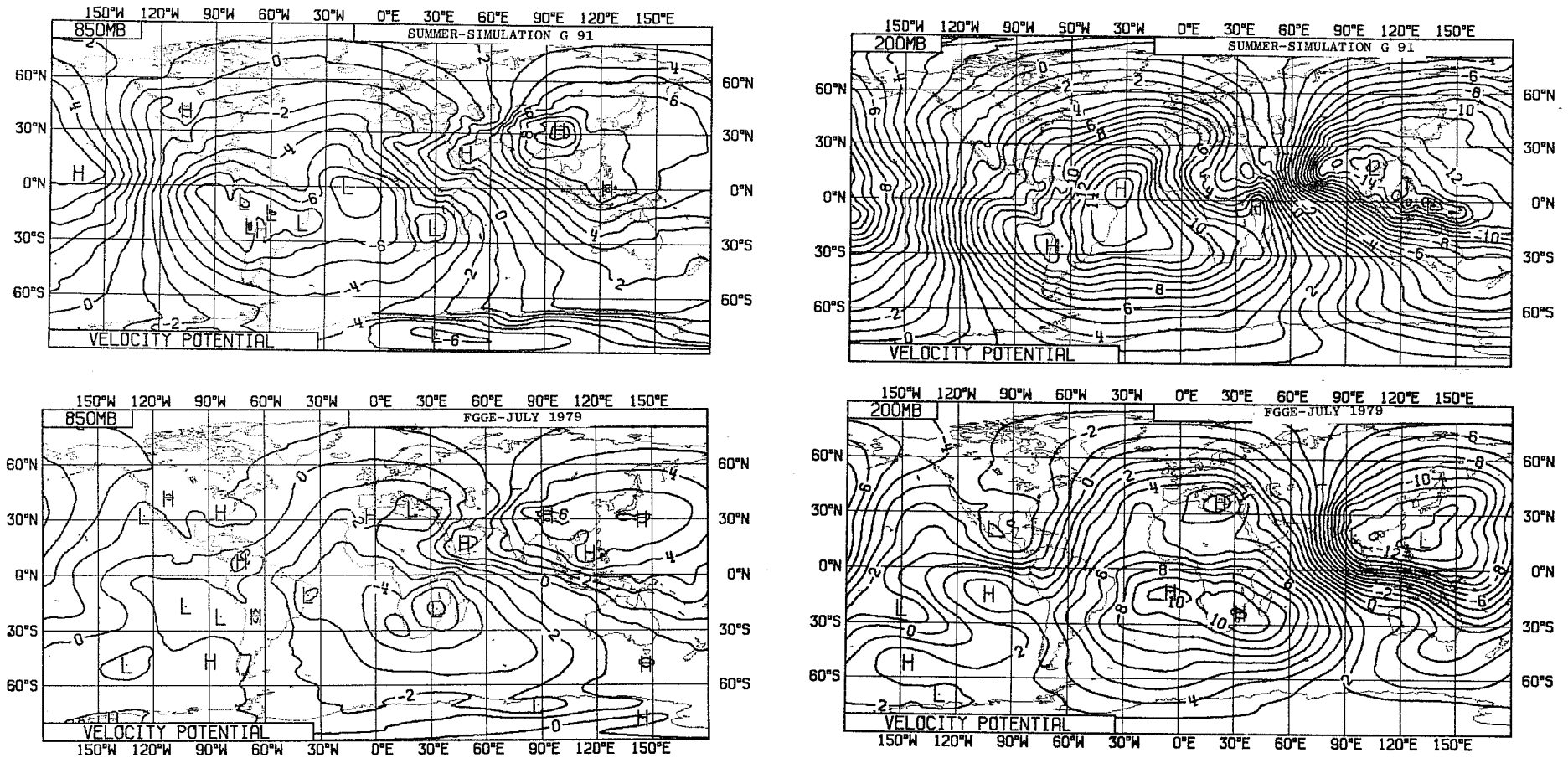

Fig. 6 Summer simulated (top) and observed (bottom) velocity potential at 850 mb and 200 mb.

4.2 The globally averaged state and the energy cycle

(a) Temperature

A noticeable difference between the simulation and reality is apparent in the globally averaged temperature of the atmosphere. The model's atmosphere cools continuously during the forecast until it reaches an equilibrium temperature at about day 35, which is 3 K below the initial value. The cooling in the early forecast period is basically due to an imbalance between the radiative cooling and the net heating by cumulus convection, large-scale condensation and surface heat exchange (Fig.7). The total heat balance after day 30 is maintained at a considerably lower rate of radiative cooling and slightly larger convective heating than initially.

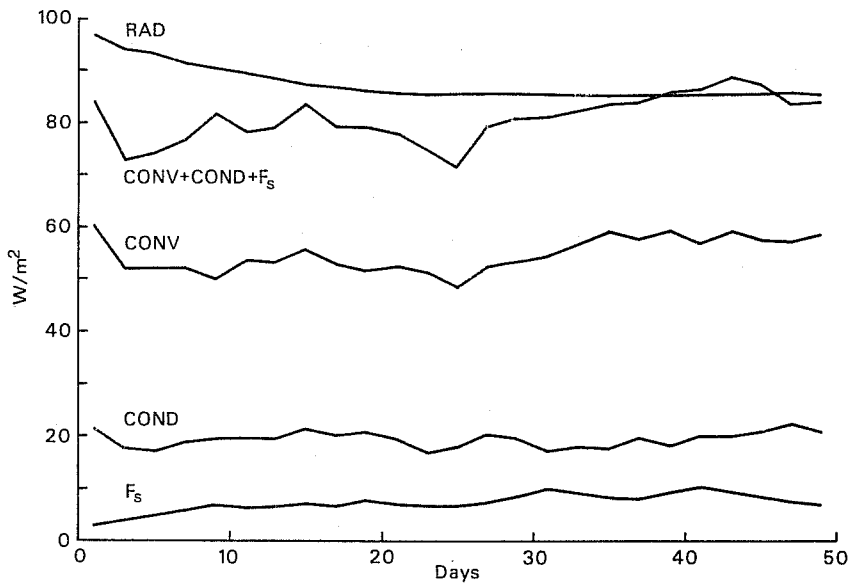

Fig. 7 Time evolution of the global mean diabatic heating rates due to radiation, convection, large-scale condensation and surface heat exchange in the winter simulation experiment G97.

(b) Energetics

Energy cycles are presented in Fig.8. The energy conversion terms are calculated directly, whereas the diabatic sources and sinks (i.e. generation of available potential energy and dissipation of kinetic energy)are obtained as residuals, assuming that potential and kinetic energies are conserved. The simulated energy cycles are compared with those calculated from ECMWF analyses for February 1982 and July 1981. Although the observed values have a large degree of uncertainty, which is, for example, expressed in the large variability of values published by different authors, the comparison clearly indicates that the simulated energy cycle significantly differs from reality. The main results are:

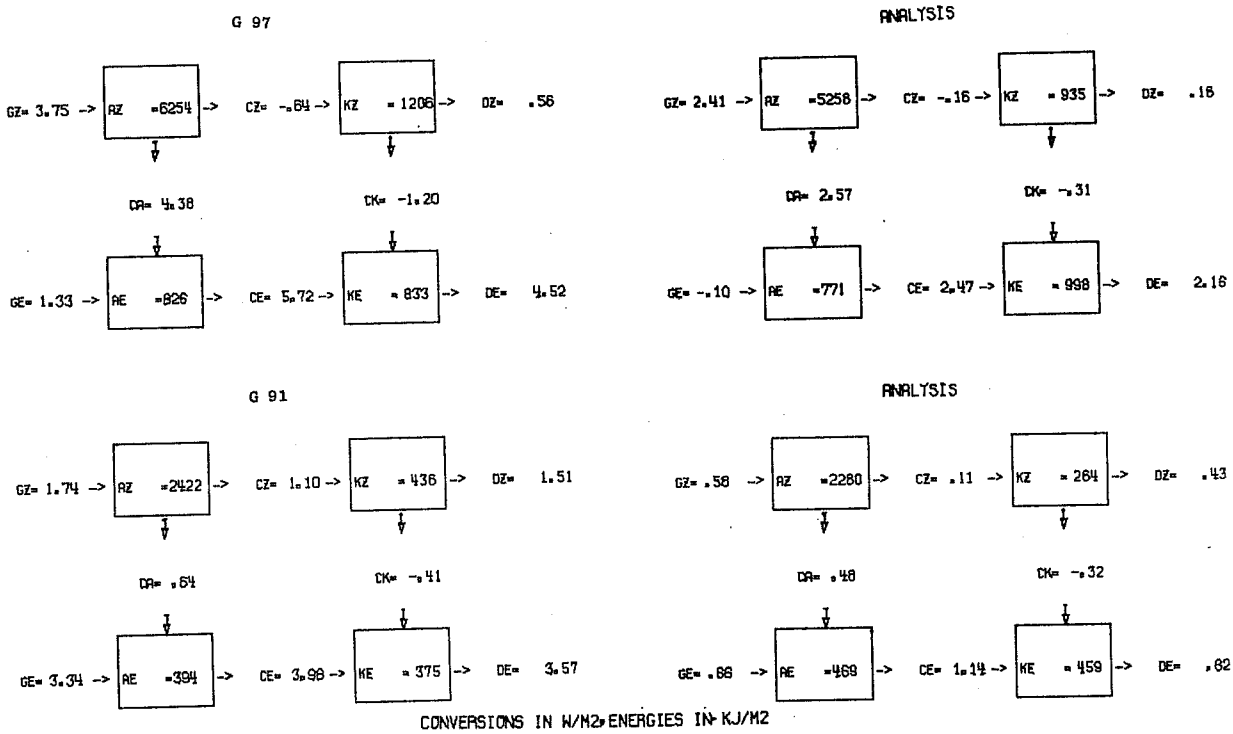

Fig. 8 Northern hemispheric energy cycle.

Top: Winter simulation (day 20-40) and for February 1982 (ECMWF analyses).

Bottom: Summer simulation (day 20-40) and for July 1981 (ECMWF analyses).

1. The eddy kinetic energy is smaller by almost one-third in the Northern Hemisphere in both seasons, whereas the zonal kinetic energy is much larger than observed (70% in summer and 40% in winter). In the Southern Hemisphere the simulated values are much closer to the observed values, although basically we find the same deficiencies.

2. The simulated baroclinic energy conversions are much stronger than observed in the Northern Hemisphere in winter and in the Southern Hemisphere in both seasons.

3. The barotropic energy conversion from eddy to zonal kinetic energy is larger than observed in the Northern Hemisphere paticularly in the winter simulation and smaller than observed in the Southern Hemisphere.

4. The diabatic generation of zonal available potential energy is also larger than observed. Besides this, we find a strong generation of eddy available potential energy by diabatic processes (with the exception of the southern hemispheric winter season) which is not confirmed by observations which support only a weak generation or even a destruction of eddy available potential energy.
   The simulated dissipation rate of eddy and zonal kinetic energy is larger in the model than observed as a result of the intensified baroclinc conversions in the simulations.

To summarize, the energy cycle appears more intense in the simulation than observed. This is particularly true for the baroclinic part of the cycle. The reasons for this increase are not clear yet. Likely causes are:

(i) The reduced static stability in the mid-latitudes due to the temperature error.

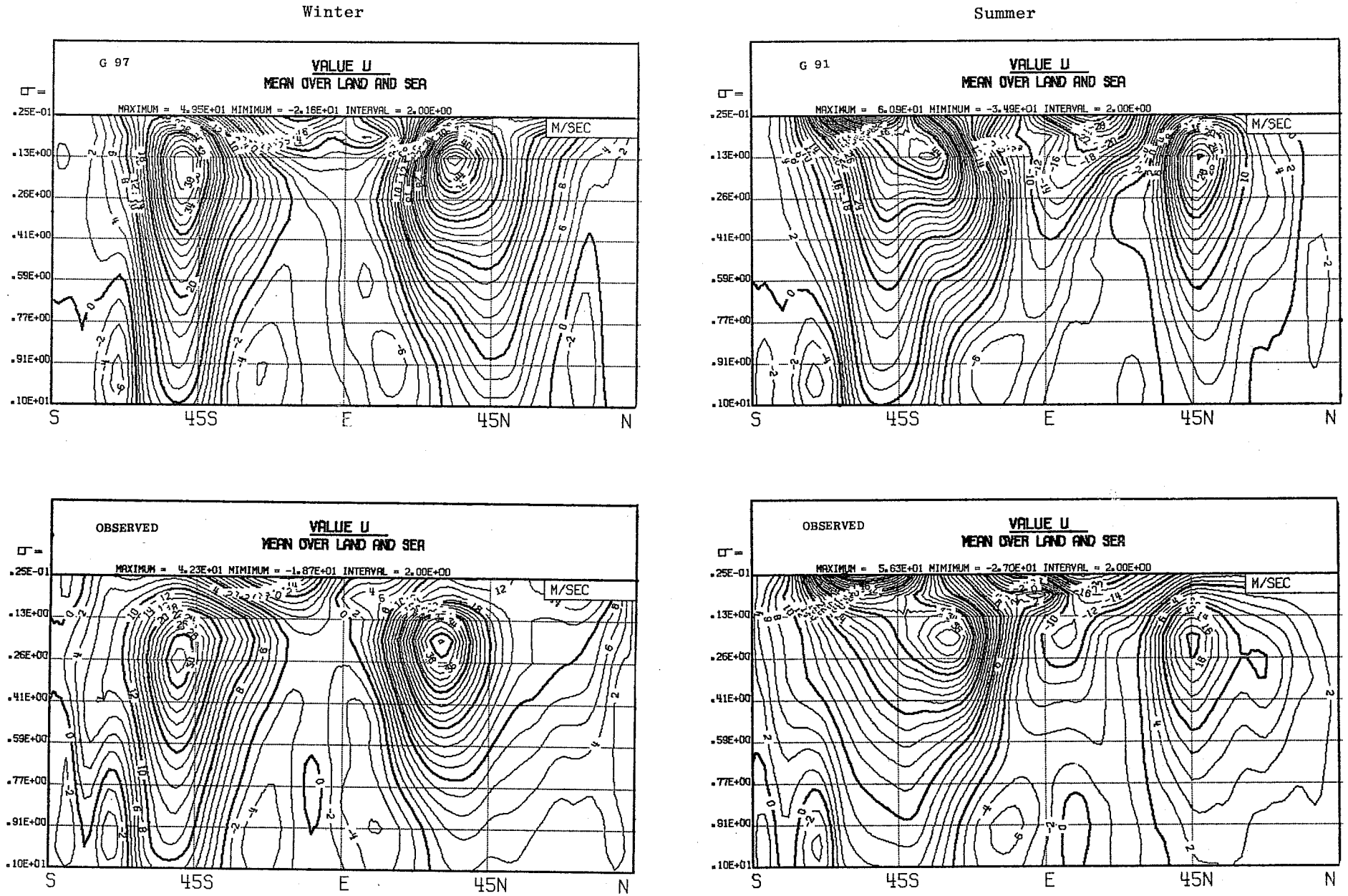

Fig. 9 Latitude-height distribution of zonal means of zonal wind component for winter and summer simulations (top) and observed (bottom) in February 1979 and in July 1979.

(ii) Increase of the zonal flow in the mid-latitudes.

(iii) Weakened standing eddies.

(iv) Erroneous diabatic forcing.

4.3 The zonally averaged flow and its forcing.

In the following section we discuss the zonally averaged flow and its forcing.

(a) Temperature

It was shown before that a serious problem in the simulations is the tendency to an overall colder atmosphere. This tendency exists at all latitudes and heights except at the lower levels near the poles (Fig.10). The temperature error increases, however, with height and reaches its maximum error of 16° and 19° respectively in the polar stratosphere. The reasons for the tropospheric cooling are not clear yet. The stratospheric cooling in the winter simulation is probably due to an underestimated poleward sensible heat transport by the long standing waves (Fig.11), whereas in the summer simulation it may be related to an excessive radiative cooling rate (Fig.14).

(b) Moisture

The latitudinal-height distribution of the simulated moisture content appears realistic but in both simulations is the moisture content smaller than observed by as much as 2-3 g/kg in the tropical and subtropical lower troposphere. The reduced moisture content is likely to affect the radiative transfer and could together with the lower temperatures explain part of the reduced radiative cooling rates during the later stages in the forecasts (see above).

(c) Zonal wind

The distribution of the zonal wind (Fig.9 and 10) is also realistic as both simulations show the subtropical jets closed off in both hemispheres as well as the correctly placed upper level easterly flow at low latitudes. We find,

however, a number of deficiencies:

1. The subtropical jets are more intense in both simulations and in both hemispheres. The increases are 6m/sec and 10m/sec respectively.
2. The subtropical jets are displaced upward and polewards.
3. The westerly wind is increased in the extratropics, extending to the surface in the winter season hemispheres.
4. The westerly winds at high latitudes are replaced by easterly winds.

The last two errors presumably reflect the overdevelopment of the Aleutian Low and the existence of the westerly flow over Europe.

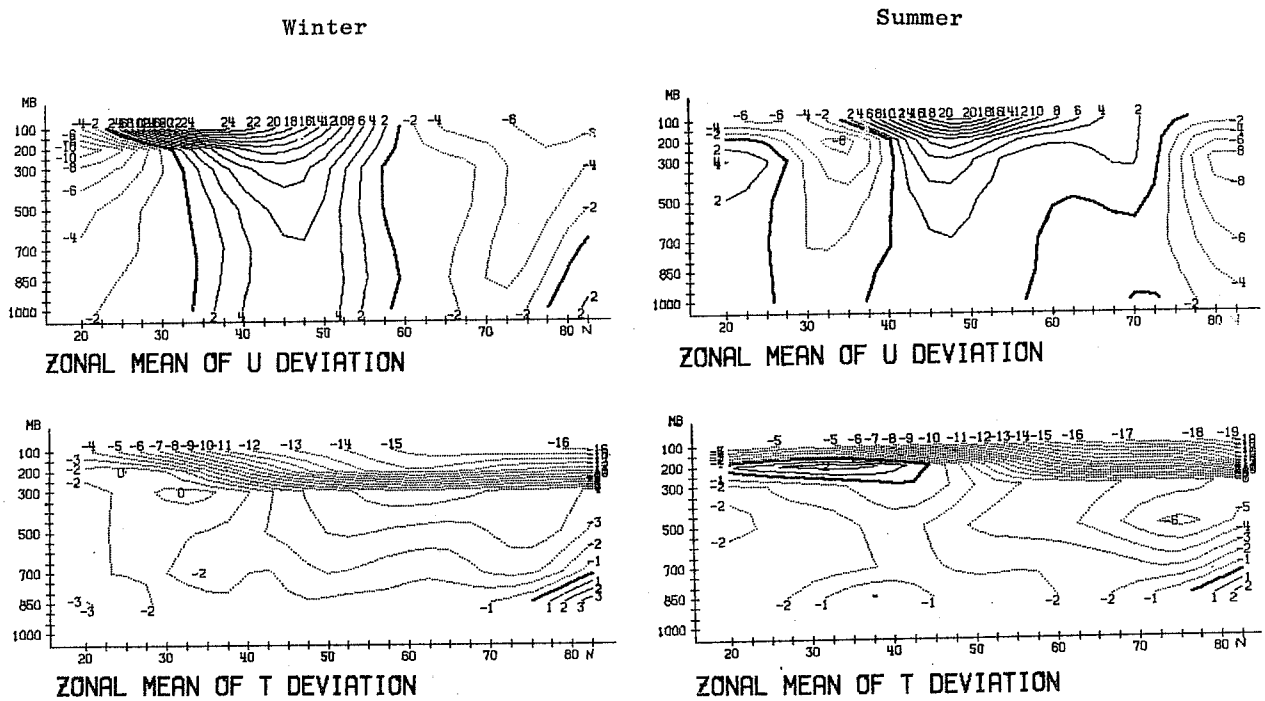

Fig. 10 Latitude height distribution of zonal means of U and T deviations from observations for the northern hemisphere.

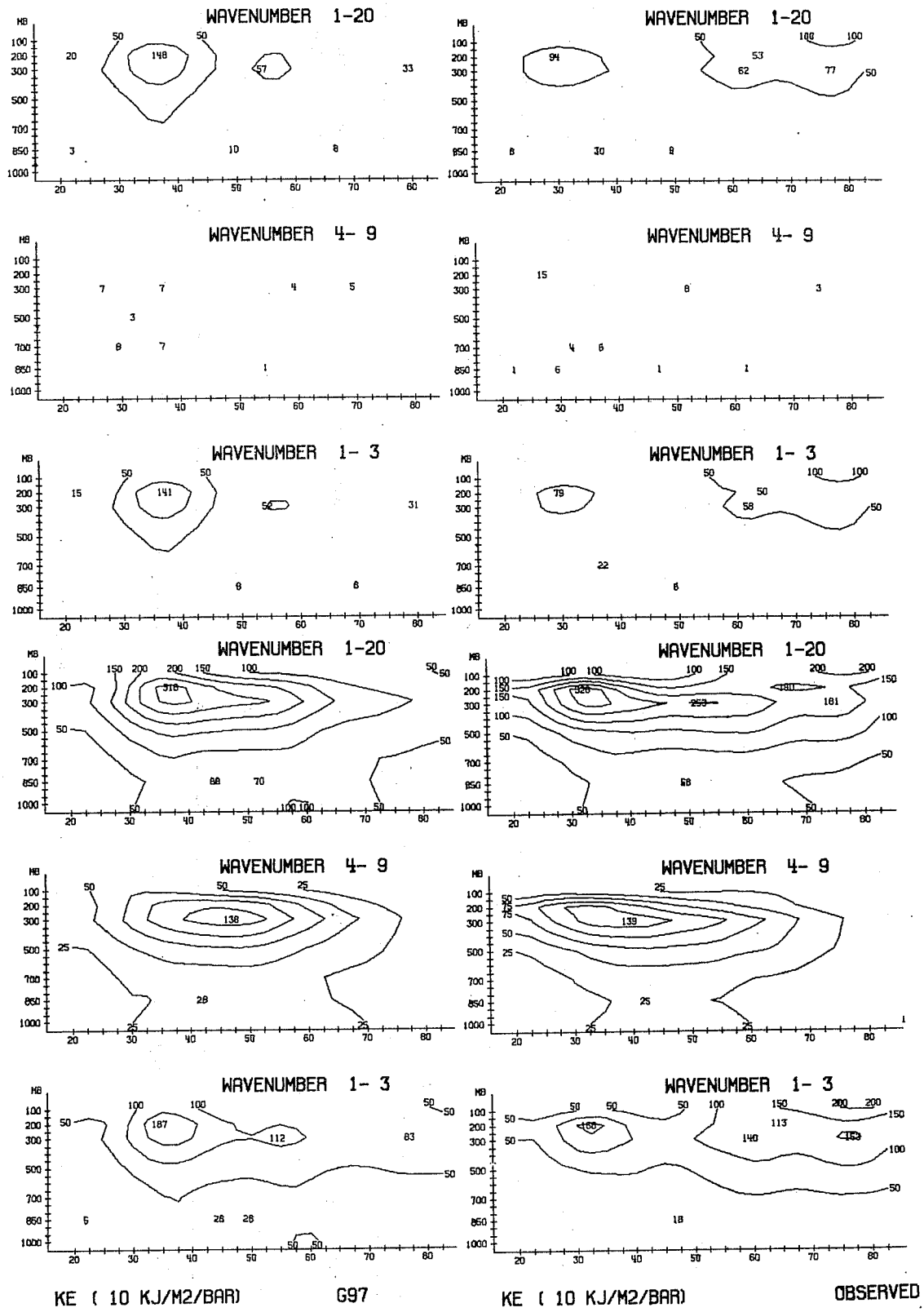

Fig. 11 Latitude height distribution of kinetic energy for different wavenumber groups for a) standing waves (top) b) standing + transient waves (bottom).

Left: Winter simulation(day 20-50)
Right: Observed 5.2-6.3.79. (FGGE).

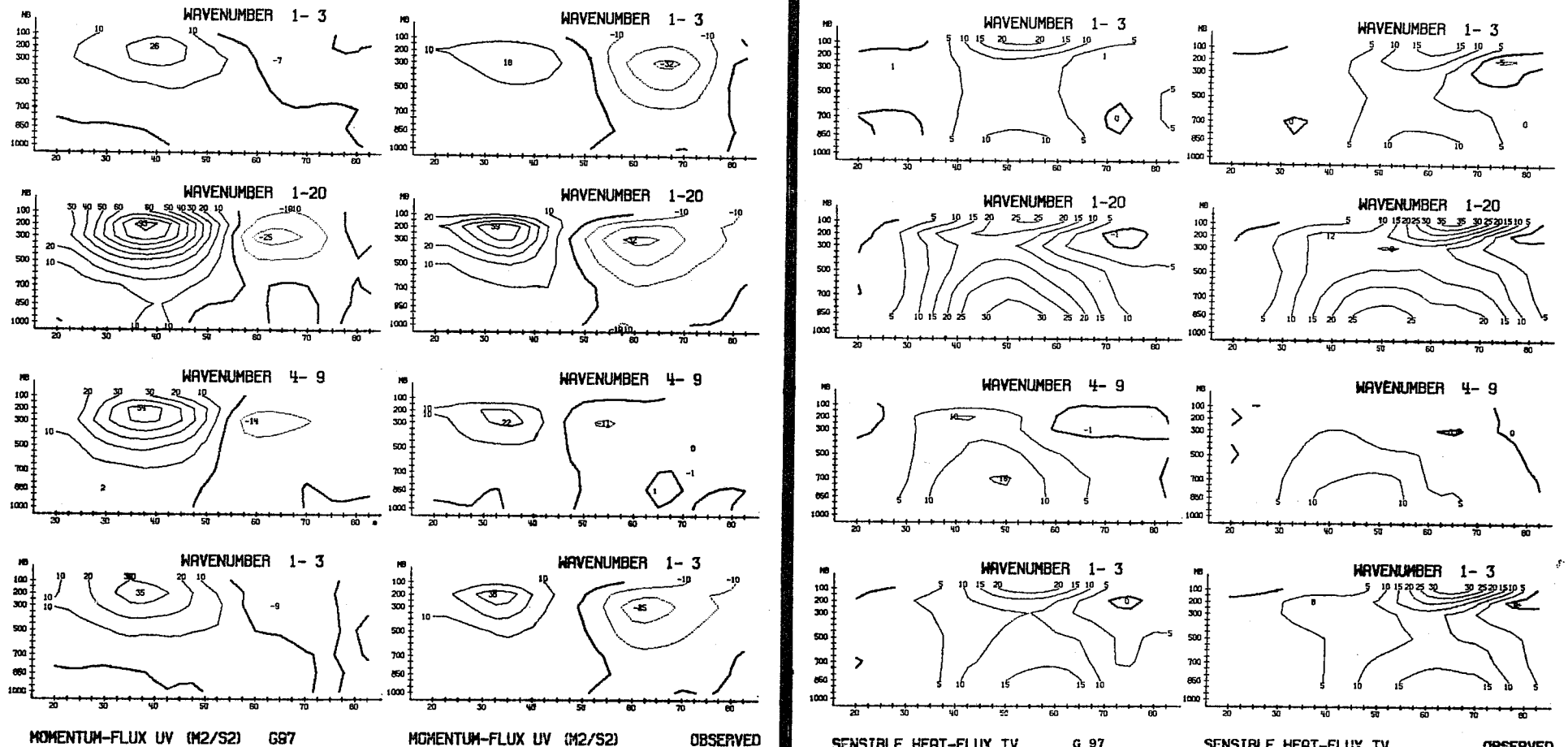

Fig. 12 Latitude height distribution of momentum flux (left) and sensible heat flux (right) for different wavenumber groups:

a) Standing waves 1-3 (top).
b) Transient + standing waves (bottom).

(d) Transient and standing eddies and eddy transport of sensible heat and momentum

In the following we study the transient and standing eddies and their northward transport of heat and momentum. Results are presented here only for the winter simulation and only for the Northern Hemisphere. The simulation is again compared with observations during the FGGE observing period.

The latitude-height distribution of the eddy kinetic energy confirms the earlier statements on the energy cycle. Although we find a fairly realistic distribution for the different wavenumber groups, the following deficiencies are evident:

1.(a) The eddy kinetic energy of the medium long waves is slightly underestimated (Fig.11, wavenumbers 4-9).

(b) Despite their reduced intensity they transport considerably more zonal momentum and sensible heat northward than observed (see Fig. 12, wavenumber 4-9).

2.(a) The eddy kinetic energy of the standing long waves is too large at the mid-latitudes but far too small at higher latitudes (see Fig.11, top).

(b) As a result of this we find that their northward momentum transport at mid-latitudes is stronger, whereas the southward momentum transport at high latitudes is severely underestimated (Fig.12). The sensible heat transport is, however, less effected; the low level and stratospheric maxima are both reproduced, although both are displaced southward by 10°. A closer examination of the single standing waves reveals that the longest wave (zonal wavenumber 1) has the largest amplitude followed by wavenumber 3, whereas wavenumber 2 is the weakest (Fig.13). This is not confirmed by observations during FGGE nor by climate values which show that wavenumber 2 is generally dominant. We also see that wavenumber 1 has a much larger tilt than observed, which implies large transports of sensible heat as was indeed found in the simulation in contrast to reality where sensible heat is mainly transported by wavenumber 2.

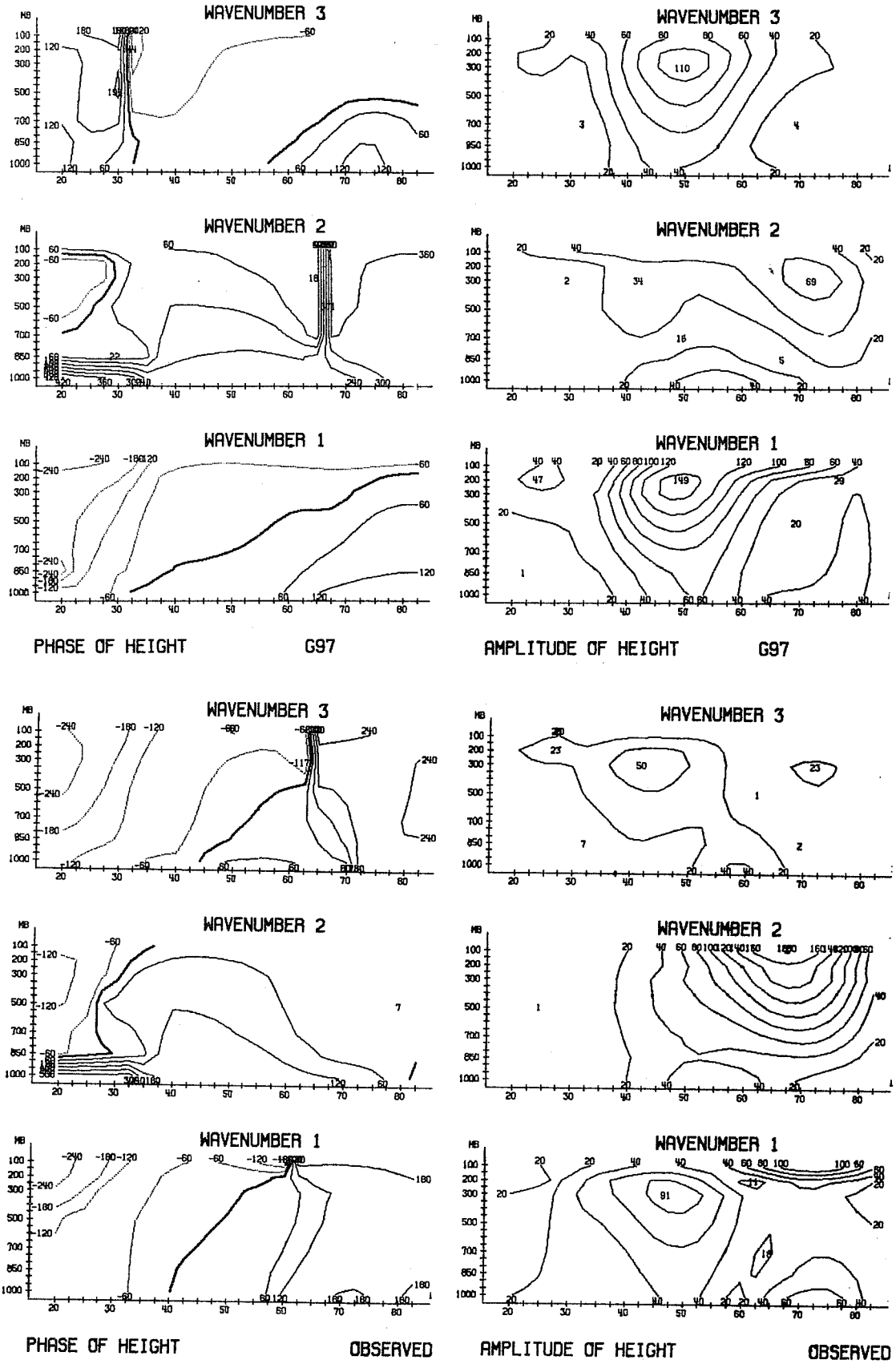

Fig. 13 Latitude height distribution of amplitude and phase of the height field for the standing waves of wavenumber 1, 2 and 3.

Top: Winter simulation (day 20-50)
Bottom: Observed 5.2-6.3.79. (FGGE).

Winter

Summer

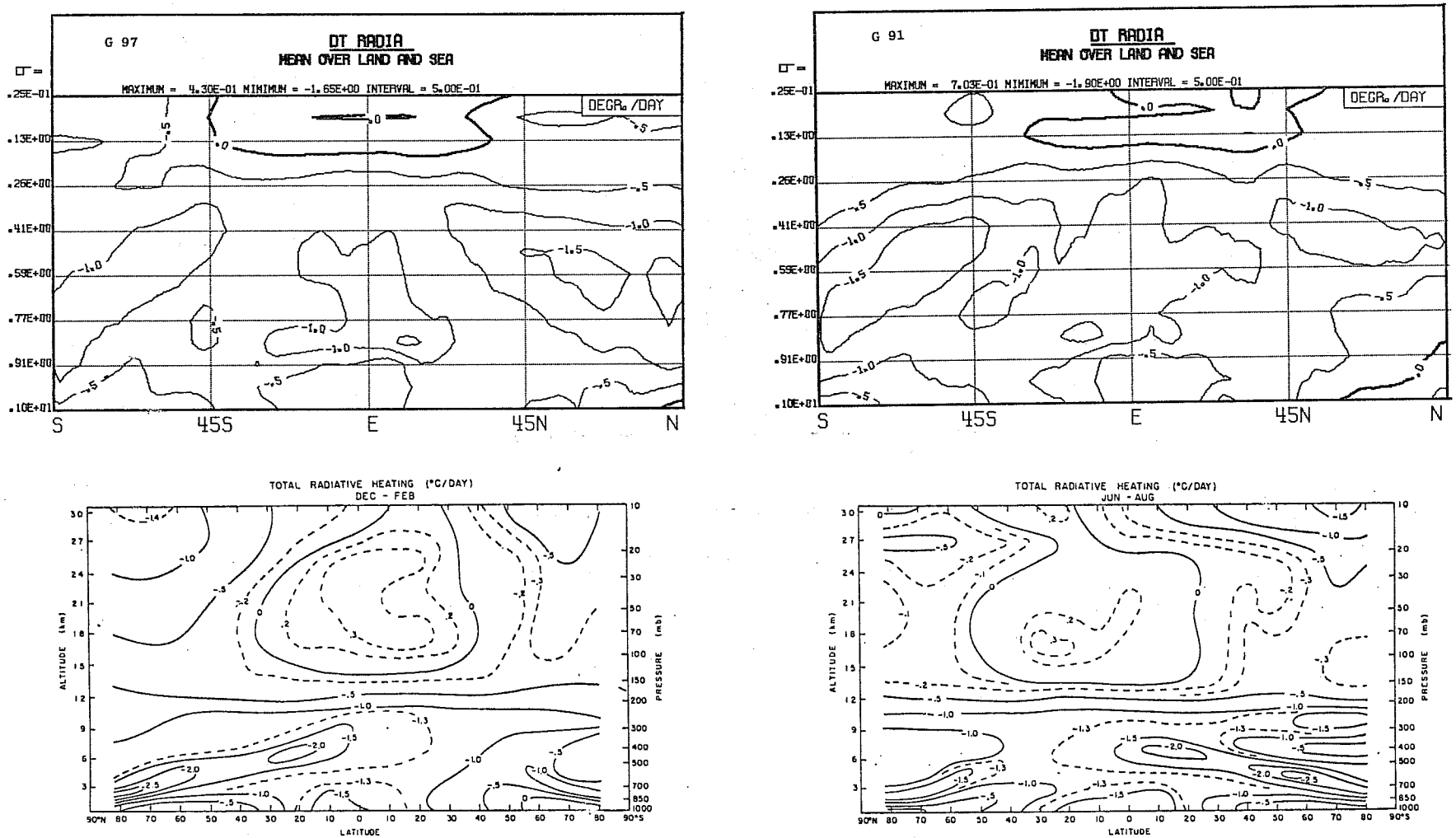

Fig. 14 Latitude height distribution of 30 day mean zonally averaged diabatic heating by radiation.

Top: Simulation (30 day mean).
Bottom: After Dopplick (1972, 1979).

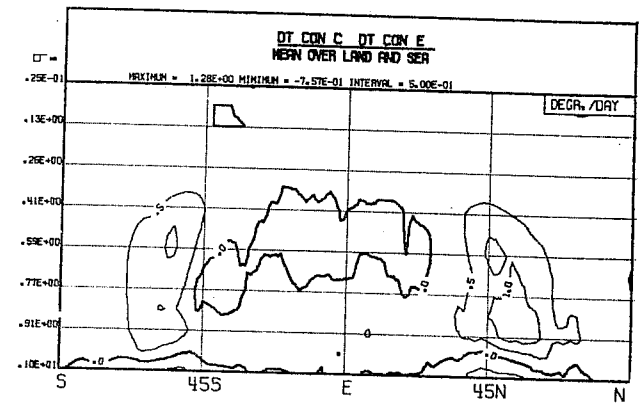

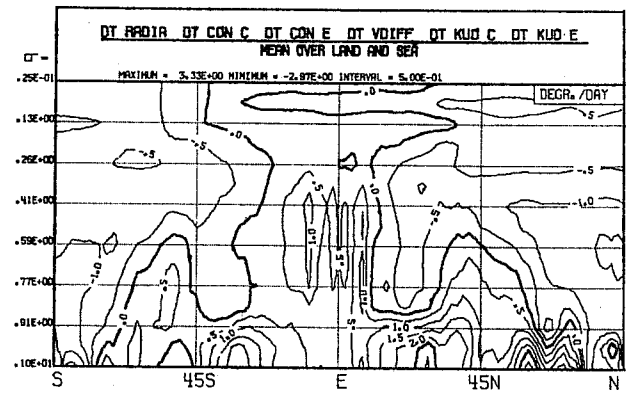

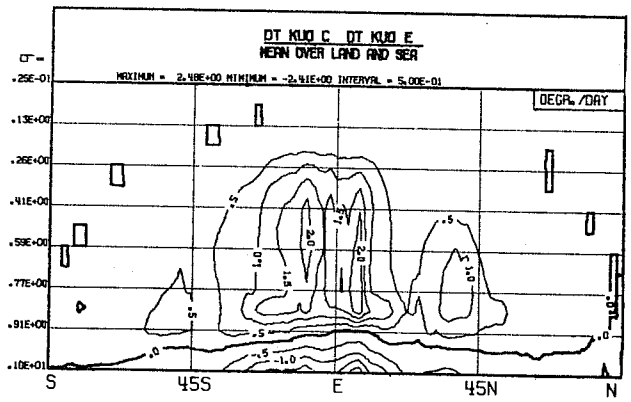

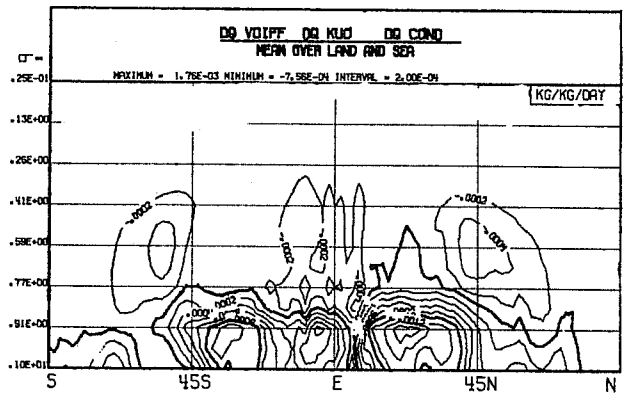

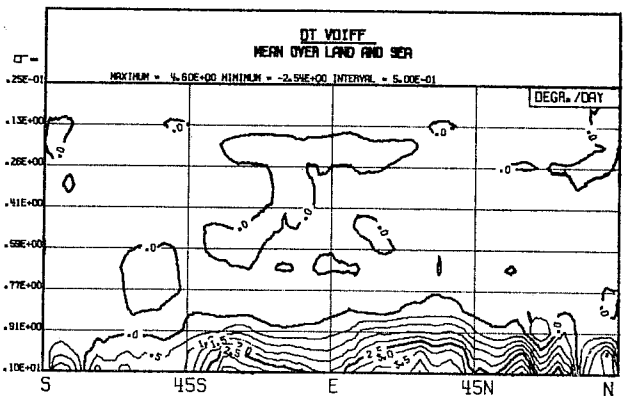

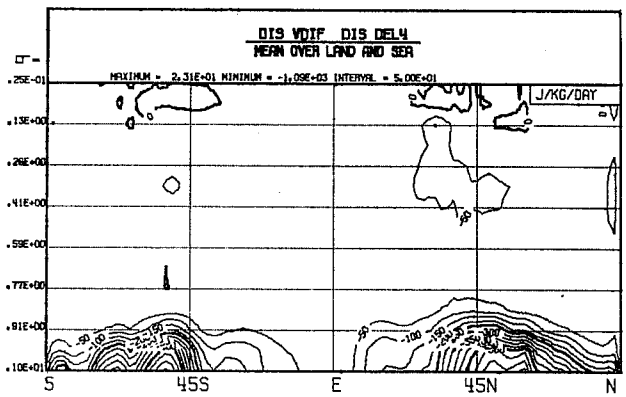

Top: Diabatic heating by large scale condensation.
Middle: Diabatic heating by cumulus convection.
Bottom: Diabatic heating by vertical turbulent heat exchange.

Top: Net diabatic heating.

Middle: Net diabatic moistening.

Bottom: Net loss of kinetic energy by vertical and horizontal diffusion of momentum.

Fig. 15 Latitude height distribution of 30 day mean zonally averaged diabatic forcing for winter simulation experiment G97.

(e) Diabatic forcing

In Figs.14,15 we present the zonally averaged diabatic forcing. Besides the net diabatic forcing for temperature, moisture and kinetic energy we also include figures of the diabatic heating by radiation, cumulus convection, large scale condensation and turbulent fluxes. Unfortunately, observations are not available for verification purposes except for radiative heating.

The latitude-height distribution of the radiative heating (Fig.14) appears realistic in both simulations. However we notice the following deficiencies which are evident from the comparison with Dopplick's estimates: underestimated cooling rates at lower levels in the tropics and near the poles and too large cooling rates in the polar stratosphere in the summer season hemispheres. The diabatic heating by the remaining processes are not verified but appear also realistic (Fig.15): the planetary boundary layer is heated by the surface heat exchange and is cooled to a lesser degree by the evaporation of rain below convective and stratiform clouds. Convective heating is largest near the equator exceeding 2°/day at some latitudes, but contributes also to the heating at mid-latitudes. The large-scale condensational heating associated with the rising air in transient eddies is dominant in the mid-latitudes and is, as we expect for a winter simulation, larger in the Northern than in the Southern Hemisphere. The simulated net diabatic heating rates (Fig.15) reveal that the atmosphere is diabatically heated at the lower levels with maximum values right at the surface. The atmosphere is further heated in the tropics, in the mid-troposphere by up to 1°/day. The simulation also produces a net heating at mid-latitudes below 600 mb. Net cooling is found elsewhere with maximum cooling rates at the North Pole.

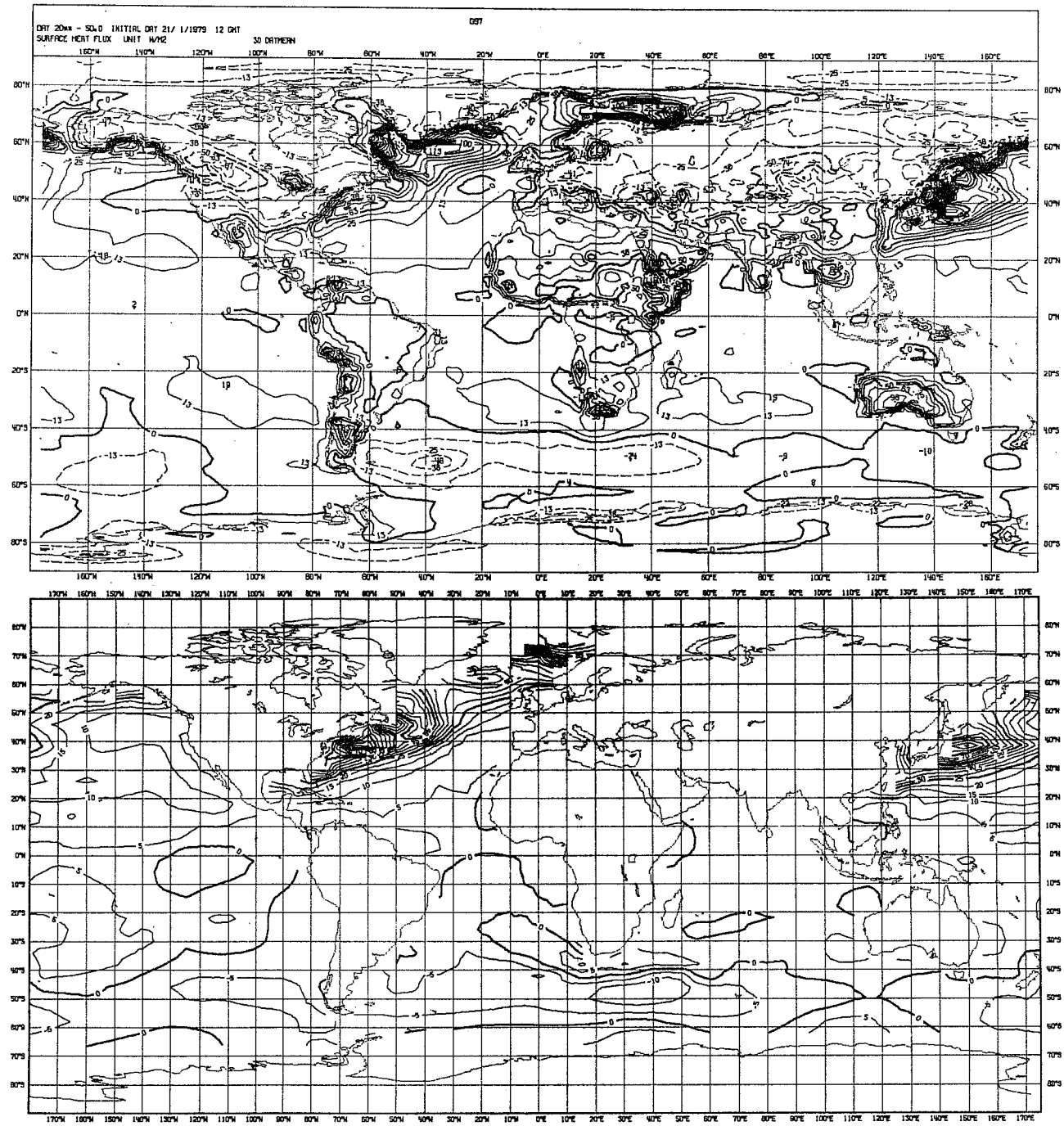

Fig. 16 Surface heat flux (W/m^2).

Top: 30 day mean of winter simulation.
Bottom: Observed values over oceans after Erbensen and Kushnir (1981).

The meridional profile of the net diabatic heating implies a net generation of zonal available potential energy, which indeed is confirmed by the simulated energy cycle (see above). The evaluation of the net diabatic heating gives, however, no indication that the generation of zonal available potential energy is larger than observed, as found in the energy cycle. To answer this question reliable data from observation would be needed.

4.4 The geographical distribution of the diabatic forcing

We consider here only the time averaged forcing for the forecast period day 20 to day 50. The forcing fields were obtained by accumulating the diabatic tendencies for the different processes as precipitation, surface fluxes etc at every grid-point for the 30-day period. The simulated forcing fields are verified against climatic data of the months February and July taken from different sources: Climate Research Institute of Oregon State University, Jaeger (precipitation), NOAA (radiation). Figs.16-22 show the global distribution of the diabatic forcing by single processes as well as the net forcing, such as net diabatic heating, net surface heat flux and net surface moisture flux.

(a) Surface sensible heat flux

The geographic variation of the surface heat exchange is remarkably well reproduced in the simulations. In agreement with observation, we find the main heat sources and sinks of realistic intensities (see Fig.16 for winter simulation).

Over the Oceans the model reproduces:

Maxima off the east coasts of Asia and North America, including its extension to the North Atlantic and the Arctic Ocean in the winter simulation.

Small upward heat fluxes in the subtropics (tradewind areas).

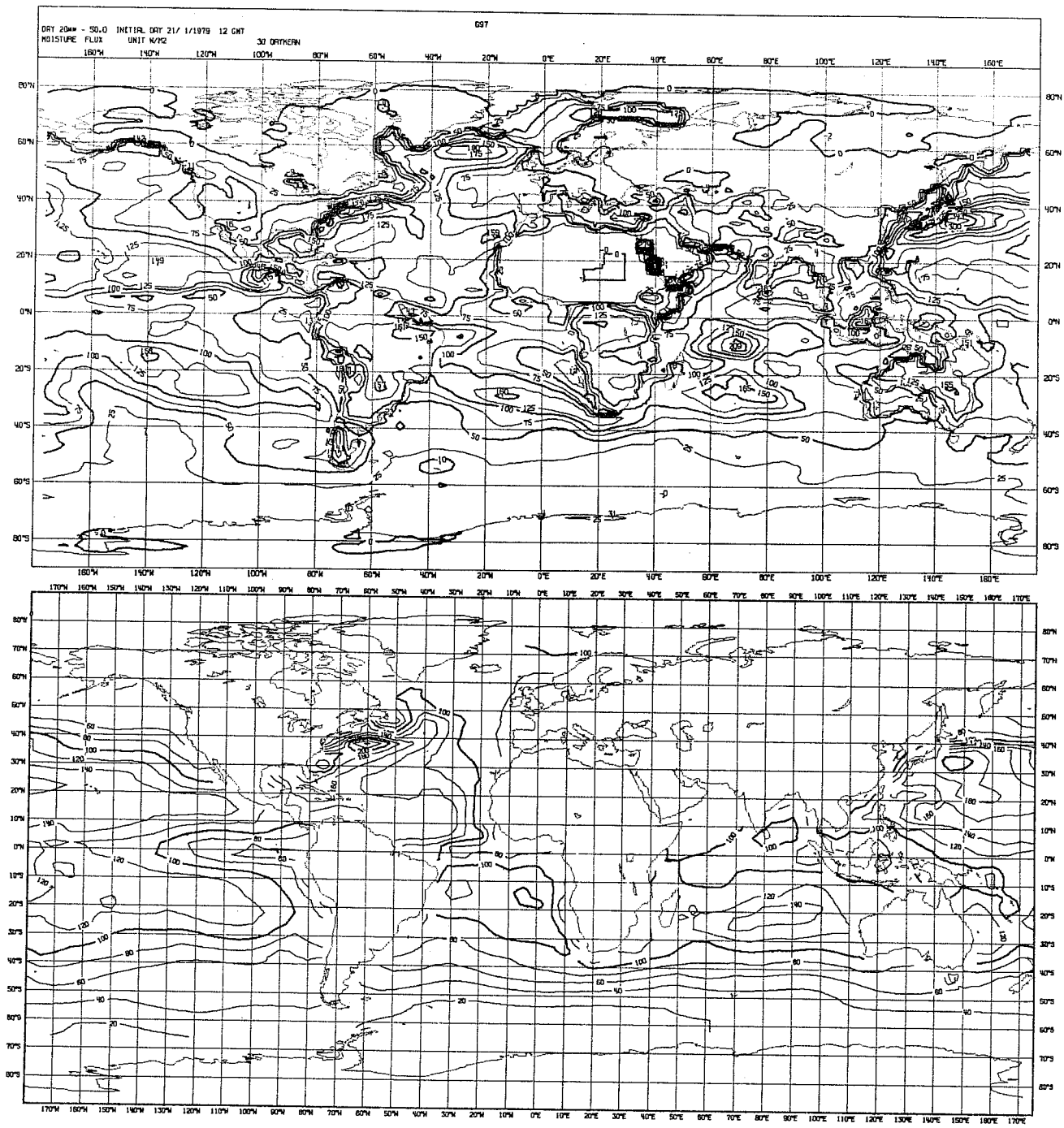

Fig. 17 As Fig. 16 but for latent heat flux (W/m^2).

Minima over the tropical oceans.

Downward fluxes over the oceans at mid-latitudes during the summer season.

Over Land we find in the simulations:

Maxima over the dry continental areas (Africa, Australia, Arabia, South of North America). For verification see Schutz and Gates (1971, 1972). Noticeable is the large heat supply to the atmosphere over Asia in the summer simulation and over the Andes and East Africa. Unfortunately, observational data are not available for these areas. The heat supply over Asia in summer may be overestimated.

(b) Surface latent heat flux

The global distribution of the surface latent heat flux also appears realistic (see Fig.17 for winter simulation). Over the Oceans we find agreement with observation:

1. Maxima of the observed intensities over the Pacific and Atlantic in the winter simulation (cold air mass transformation).

2. Maxima in the subtropics in the tradewind areas, and smaller fluxes over the tropical oceans. The minimum over the Pacific along the ITCZ is even more pronounced in the simulation than observed. The moisture supply over the Atlantic is underestimated, which also agrees with the missing ITCZ in the simulation.

3. Small moisture fluxes over the upwelling cold water off the western coast of America and Africa.

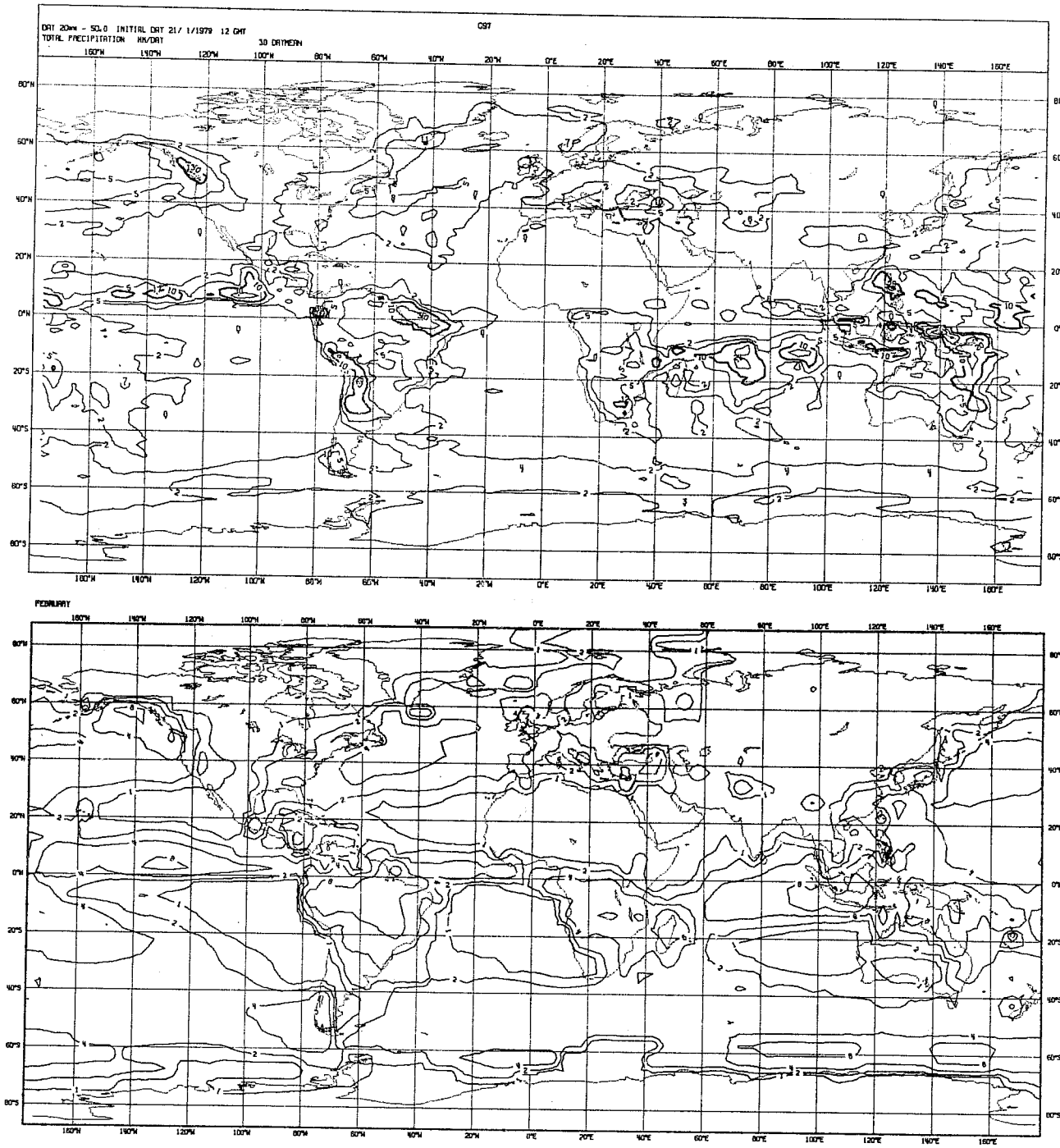

Fig. 18a Winter simulated precipitation rate (mm/day) for 20-50 day period (top) and observed mean precipitation for February after Jaeger (1976).

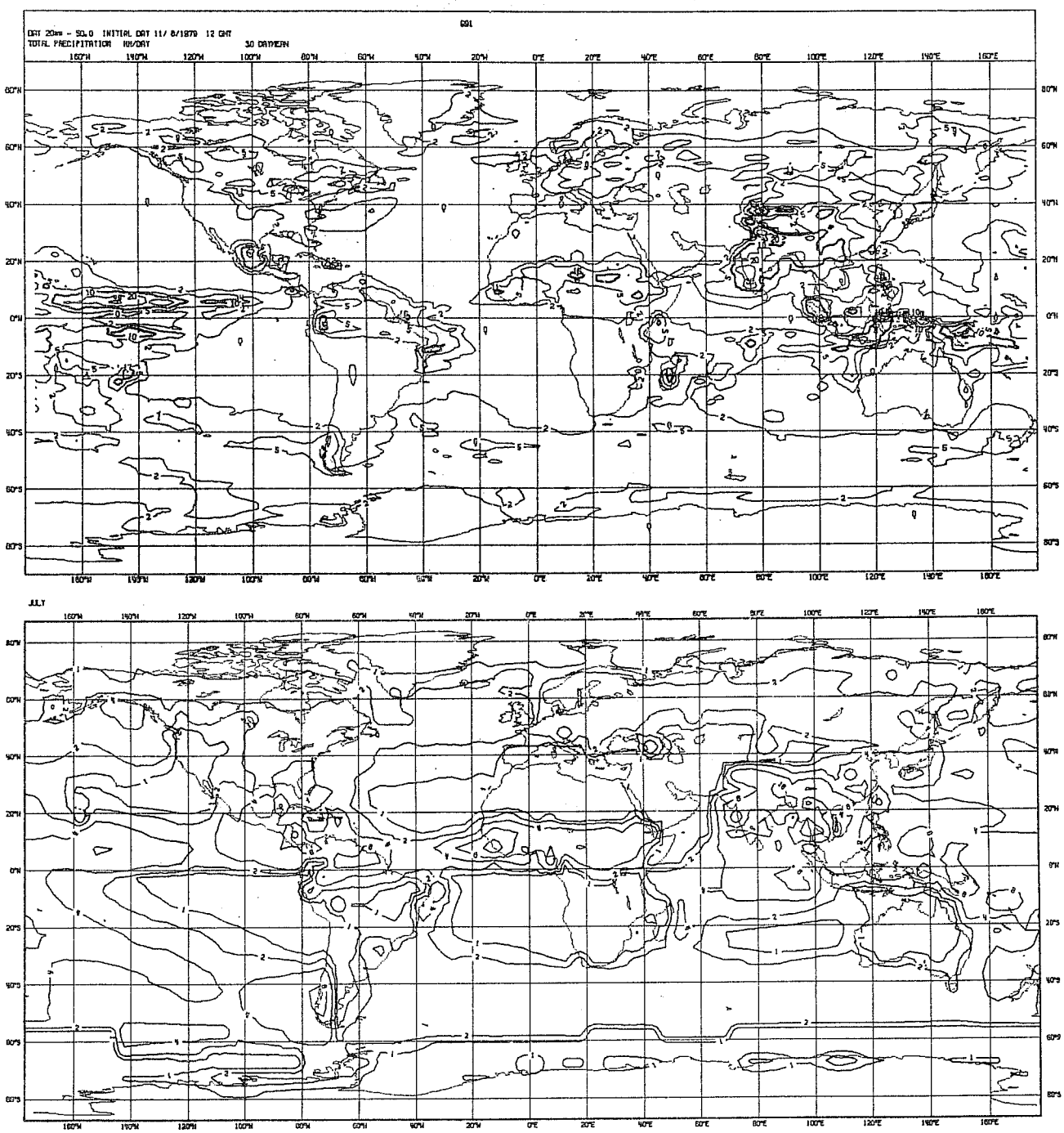

Fig. 18b As Fig. 18a but for summer simulation (top) and for July (bottom).

No verification is available over land. The distribution of fluxes, however, appears realistic as they are small over dry continental areas and large over the tropical forests (max. 150 W/m^2).

(c) Precipitation

The simulated global distribution of precipitation appears realistic when compared to Jaeger's (1976) climate values for February and July (Fig.18). The simulations reproduce the main climatological features as:

Minima over the subtropical oceans.

Sharp maxima along the ITCZ over the Pacific which is, however, overestimated in the winter simulation.

Location and intensity of maxima over the tropical continents.

Monsoon rainfall over India (too strong).

Maxima over Indonesia and over the Indian ocean south of the equator are present but are too strong (consistent with the too-intense divergent flow in that area, as shown above).

Extratropical maxima along cyclone tracks over the oceans and eastern parts of the continents.

The ITCZ over the Atlantic is, however, absent in the winter simulation and is too weak in the summer simulation (consistent with the weaker moisture supply over the Atlantic tradewinds).

(d) Net surface heat flux

The net surface heat flux

$$G_S = R_S - H_S - L.E_S$$

represents the gain or loss of heat of the ocean or land by radiative fluxes and by the fluxes of sensible and latent heat. As the ocean temperature can be assumed constant or slowy varying in time, a non-zero heat flux reflects the transport of heat by ocean currents, whereas non-zero heat fluxes over land imply changes of the surface temperature. From Fig.19 we see that the heat fluxes balance fairly well over land in the simulations except over North Africa, Australia and parts of North America. In fact, a significant increase in the surface temperature was observed for those areas during the forecast period. The reasons for the imbalance over the dry subtropical continents are not clear but could be associated with our radiation scheme, or the absence of the daily cycle. The imbalance over North America in winter is due to the advection of warm air by transient eddies crossing the Rockies.

The simulated net flux differs considerably from the observed flux over large areas of the tropical and subtropical oceans; the net downward heat flux off the western coasts of Africa and South America, for example, is almost twice as large as observed, which is due to 1) an excessive insolation due to the lack of low level stratiform clouds in the simulations there and 2) due to smaller evaporation rates in those areas.

The large upward fluxes over the western parts of the Pacific and Atlantic in the winter simulation which reflect the intense sensible and latent heat fluxes during cold air outbreaks are well simulated.

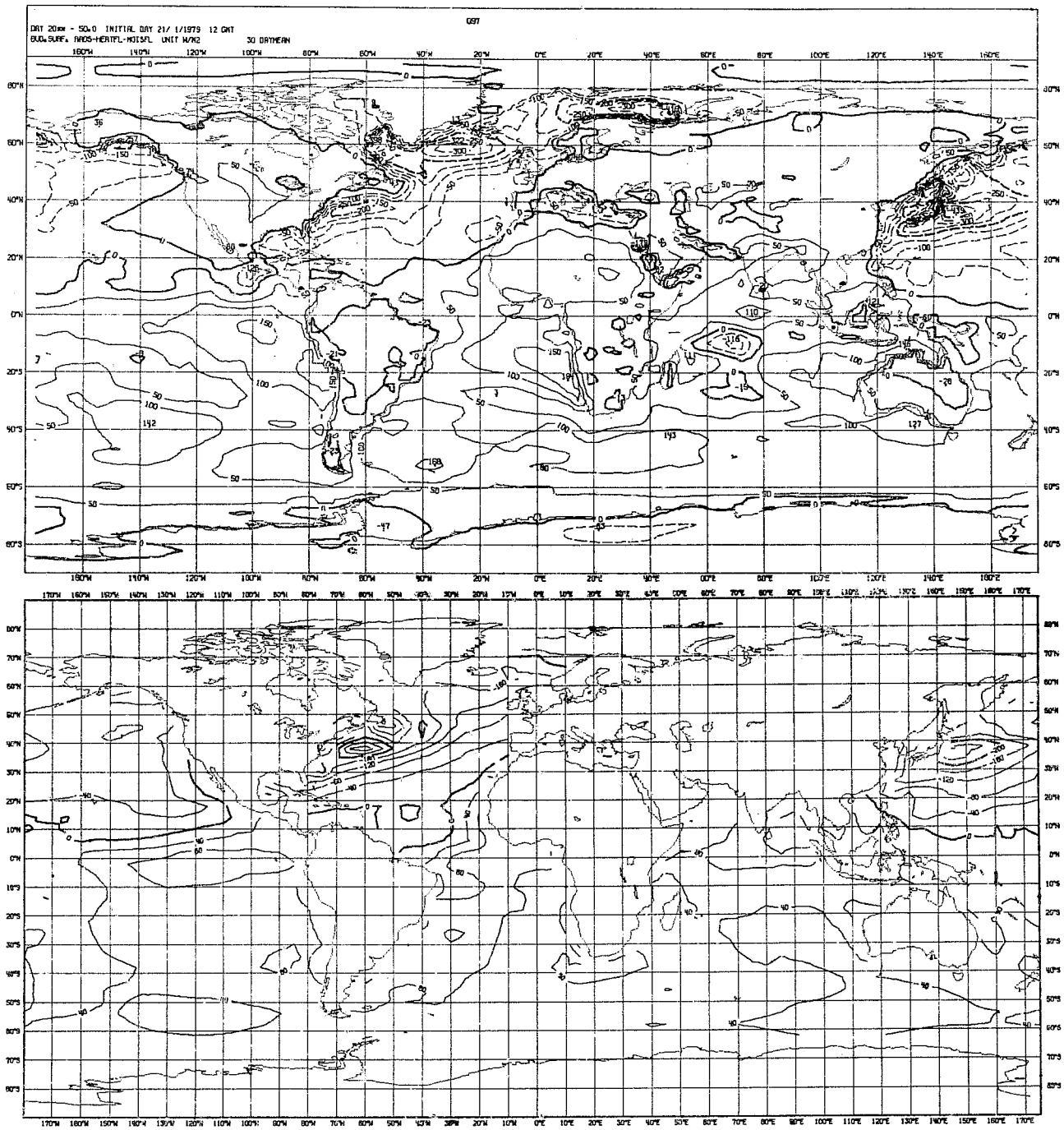

Fig. 19 As Fig. 16 but for net surface heat flux (W/m^2).

(e) Net surface moisture flux

Since moist processes play a dominant role for the atmospheric circulation, the verification of the hydrological cycles in general circulation simulations is one of the main tasks. Of particular significance is the net surface moisture flux:

$$D = P - E$$

(P = Precipitation, E = Evapotranspiration)

as it describes the net moisture exchange between atmosphere, oceans and continents respectively. In long term averages the net surface moisture flux must equal the discharge by ocean currents or run-off by streams and rivers. Unfortunately, no observational data of the net surface moisture fluxes are available except for annual mean values of discharge/run-off recently published by Baumgartner (1981). The global fields of the simulated net surface moisture flux (Fig.20) show that:

1. The bulk of moisture is supplied from the subtropical oceans and comparably small amounts from the North Atlantic, Arctic Ocean and Pacific off the east coast of Asia in the winter simulation, and from the North American continent and South Europe and Asia in the summer simulation. The values over the subtropical oceans agree well with the annual mean values by Baumgartner (1981).

2. Areas of atmospheric moisture sinks are:
   The eastern parts of the cyclone tracks.
   ITCZ over the Pacific and Indian Ocean.
   Indonesia and Western Pacific.
   Tropical continents of South America and Africa, India and Himalayas in the summer simulation.

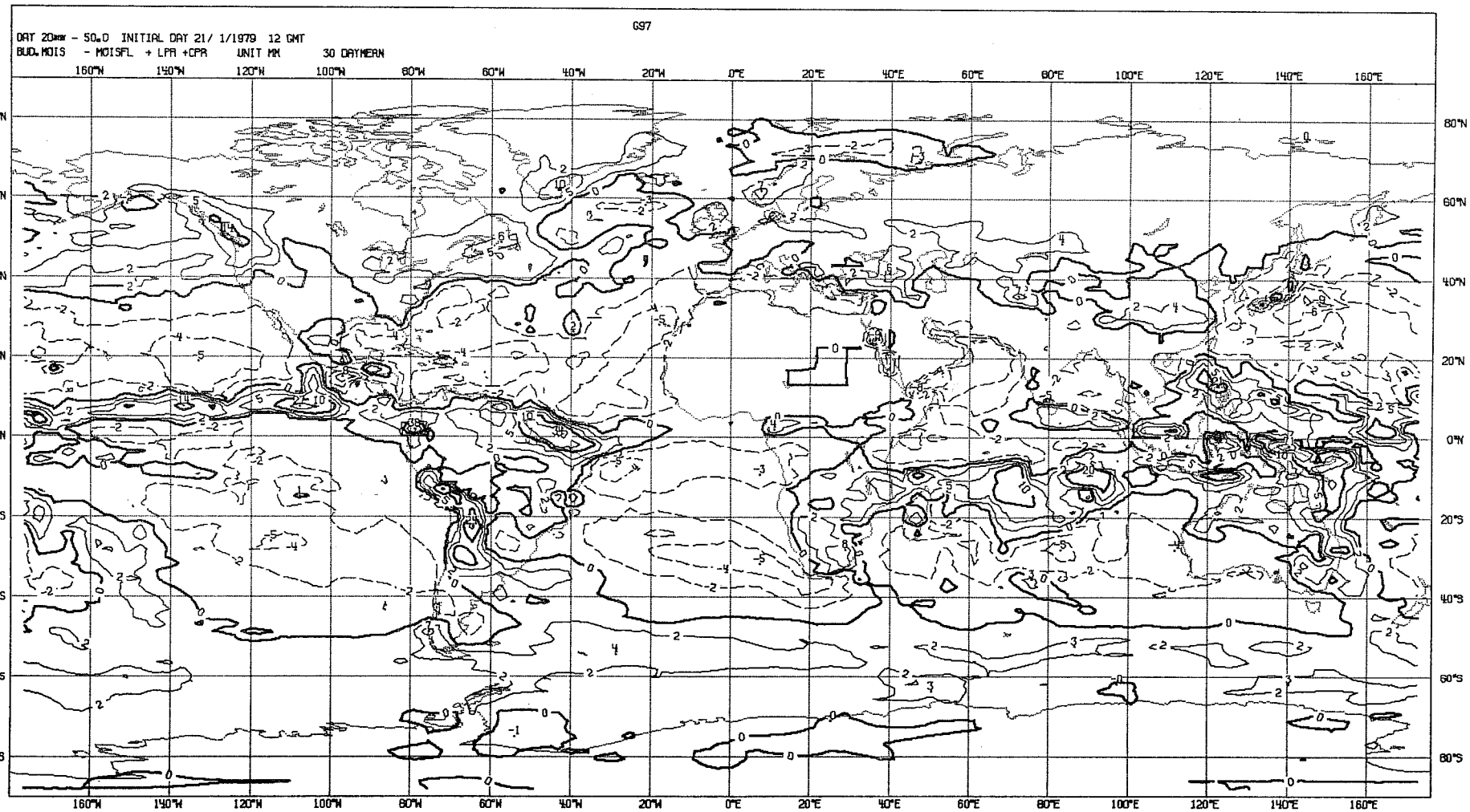

Fig. 20 Winter simulated net surface moisture flux P-E in mm/day.

We also notice that the fluxes are much larger and spatially more confined in the low latitudes than at higher latitudes. The large moisture sink in the Indonesian area and over the western Pacific is not present in Baumgartner's annual means and probably reflects the above-mentioned model's tendency to over-intensify the circulation in that area.

(f) Surface stress

Only the magnitude of the surface stress is diagnosed in the model and verifications are only available for the oceans. Simulated and observed surface stress (Figs.21) only agree well with regard to their geographical distribution, i.e. they have maxima along the cyclone tracks and over the tradewind areas. The intensity of the surface stress is badly simulated; in the extratropics the surface stress exceeds the climate values by as much as 100% in places. This excess is consistent with the model's too intense energy cycle described earlier. The intensity of the surface stress is fairly realistic in the tradewind region over the Pacific and Indian Ocean, but is underestimated over the Atlantic particularly in the summer simulation. The strong maximum over the Indian Ocean during summer is also present in the simulation but less intense than observed.

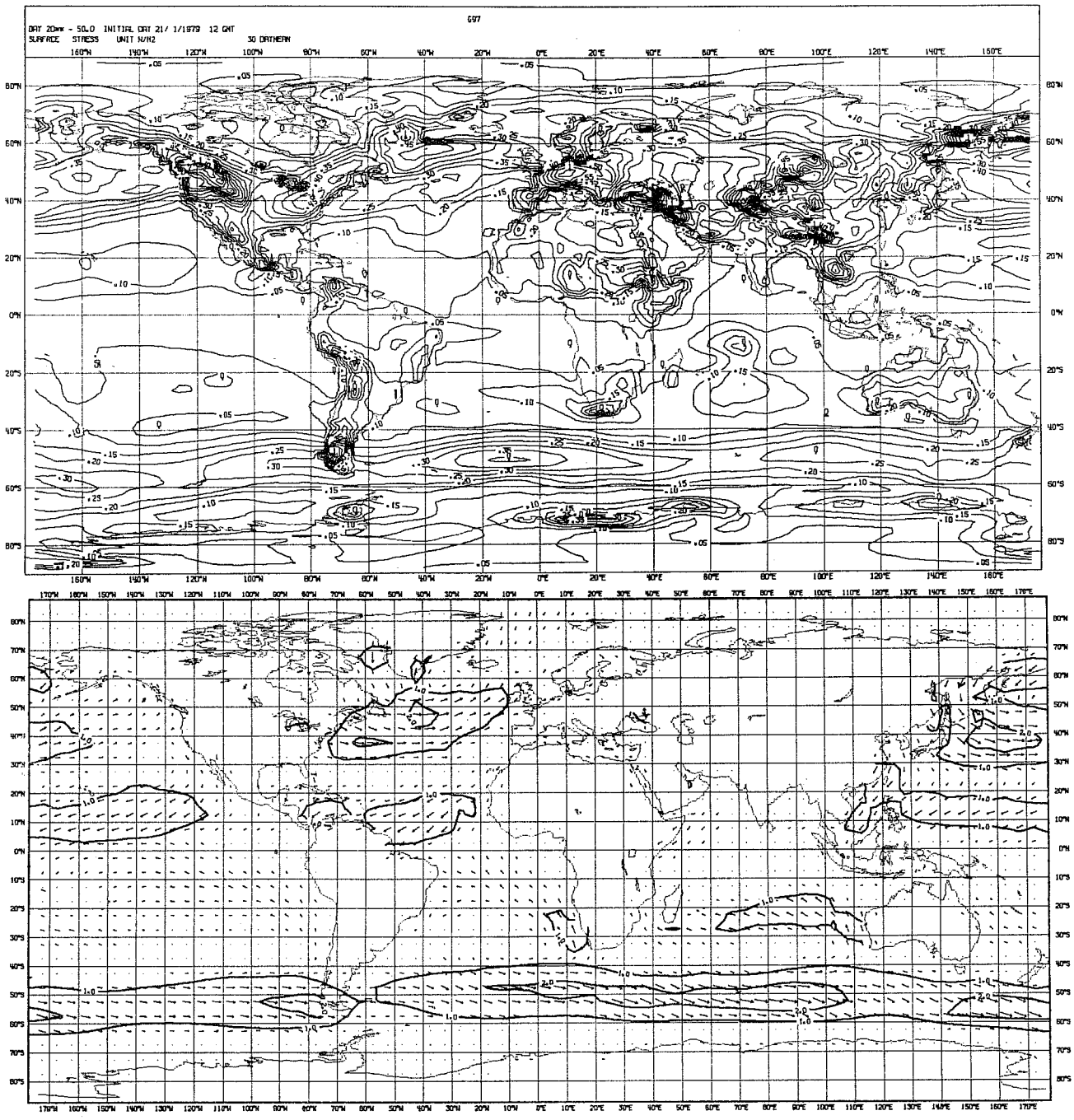

Fig. 21 Surface stress.

Top: 30 day mean of winter simulation (N/m^2).
Bottom: Observed values over oceans after Han and Lee (1981) (0.1 N/m^2).

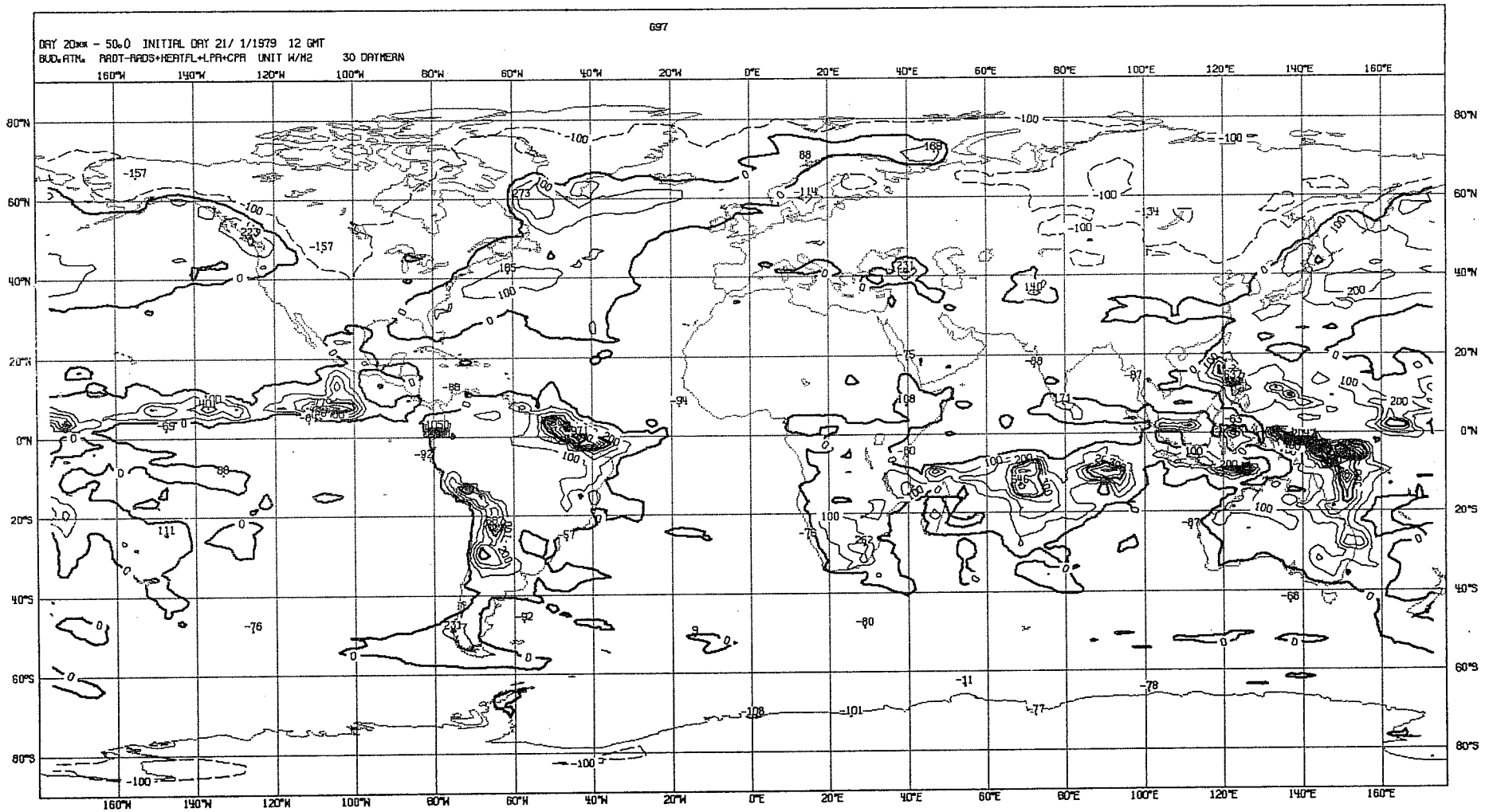

Fig.22a Winter simulated vertically integrated net diabatic heating rate (in W/m^2).

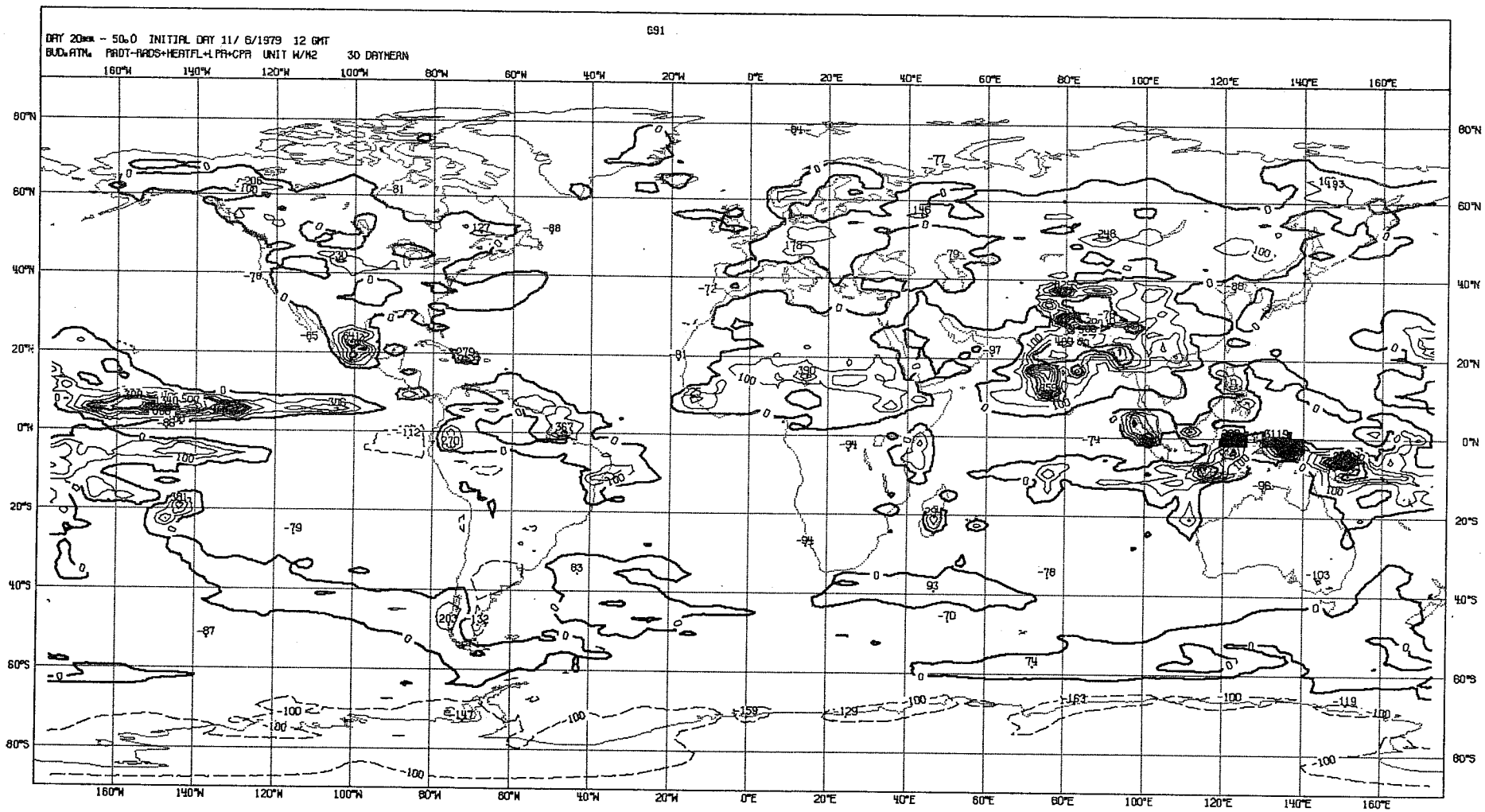

Fig. 22b Summer cimulated vertically integrated net diabatic heating rate (in W/m^2).

(g) Net adiabatic heating

The vertically integrated net diabatic heating due to radiative processes, condensational processes and surface heat exchange is displayed in Fig.22. Although observed fields for verification purposes are not available, the geographical distribution of heat sources and sinks appears very realistic. Since the longitudinal variation reflects mainly the spatial distribution of precipitation and surface heat fluxes we find the main heat sources in the following areas:

(i) Along the ITCZ over the Pacific and Indian Ocean (both simulations).

(ii) Indonesia and western Pacific (both simulations).

(iii) India and the Himalayas in the summer simulation.

(iv) Atlantic and Pacific of the eastern coasts of North America and Asia respectively in the winter simulation.

(v) The seasonally changing rainbelts of South America and Africa.

(vi) Europe, Asia and North America in the summer simulation.

As we might expect, the diabatic cooling covers much larger areas and is therefore much smoother.

Neither simulation produced a heat source over the tropical Atlantic, which is presumably linked to the underestimated moisture supply in the tradewind area over the north Atlantic.

Although the strength of the net heat sources and sinks cannot be verified at present, our evaluation of the simulated diabatic forcing indicates that the heat source over Indonesia and the western Pacific is too intense.

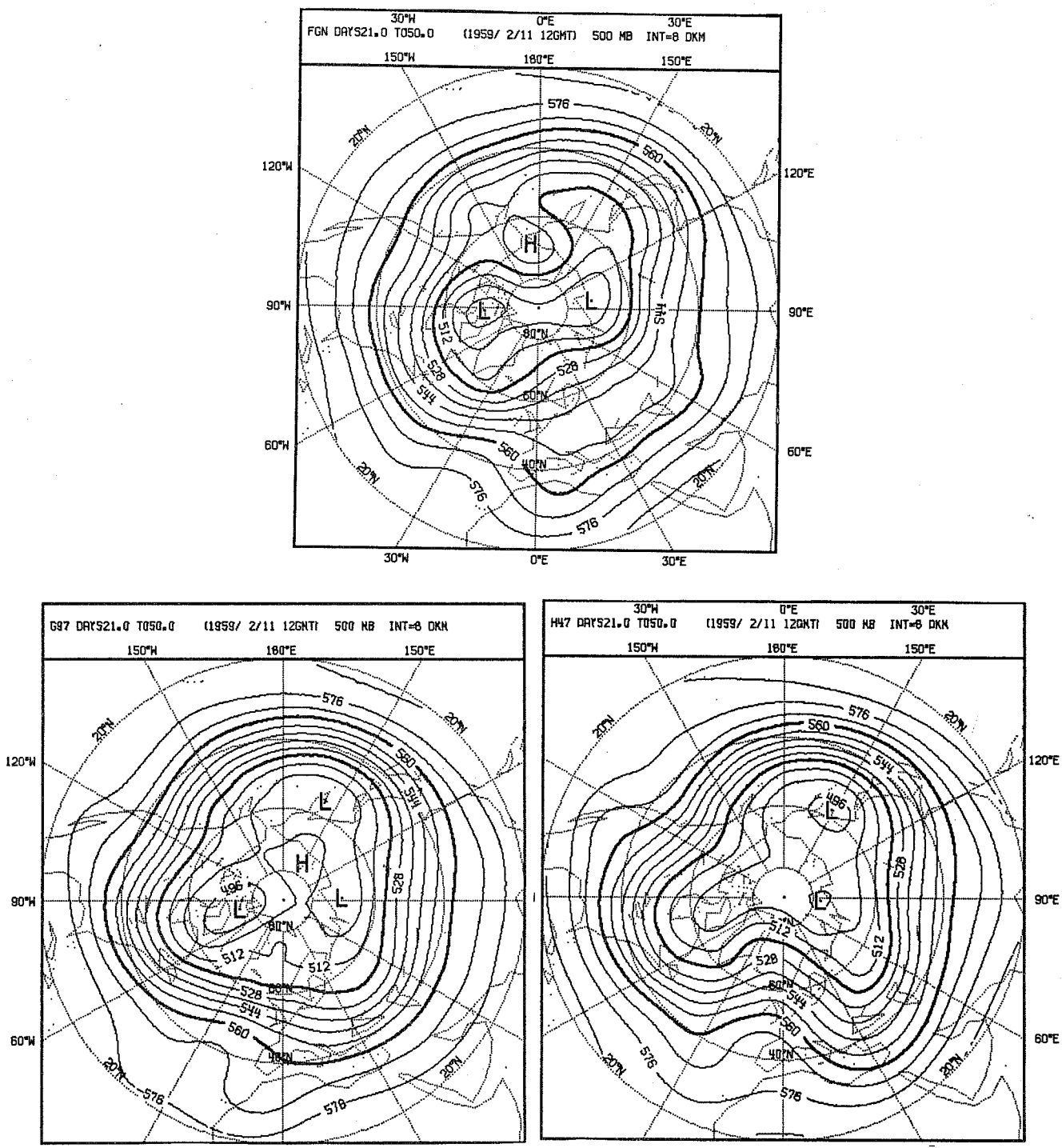

Fig. 23 30 day mean 500 mb heights.

Top: Observed in February/March 1979.
Bottom: Simulation with Kuo (left).
Simulation with A-S (right).

5. AN EXPERIMENT TO STUDY THE SENSITIVITY OF THE MEAN SIMULATED FLOW TO THE PARAMETERIZATION OF CONVECTION

In this last section an experiment is described which was performed to study the sensitivity of the simulated mean flow to the parameterization of convection. A winter simulation experiment was therefore repeated where the standard Kuo-convection scheme is replaced by a version of the Arakawa-Schubert scheme (Arakawa-Schubert, 1974) developed at the Centre. The main results are briefly summarized in Figs.23-27.

We find large differences in the simulated mean flow in the tropics as well as in the extratropics, most noticeable over the Eastern Atlantic and Western Europe, where we find a strong ridge of high pressure in the new run which is absent in the control run and which is also present though weaker in the observation. The existence of this intense ridge in the mean flow seems to be teleconnected to the large heat source over South America which is associated with deep convection (Fig.26). The existence of this teleconnection is further confirmed by studying the difference of the 200 mb streamfunction of both runs which show a wave-like pattern structure between both areas (Fig. 24).

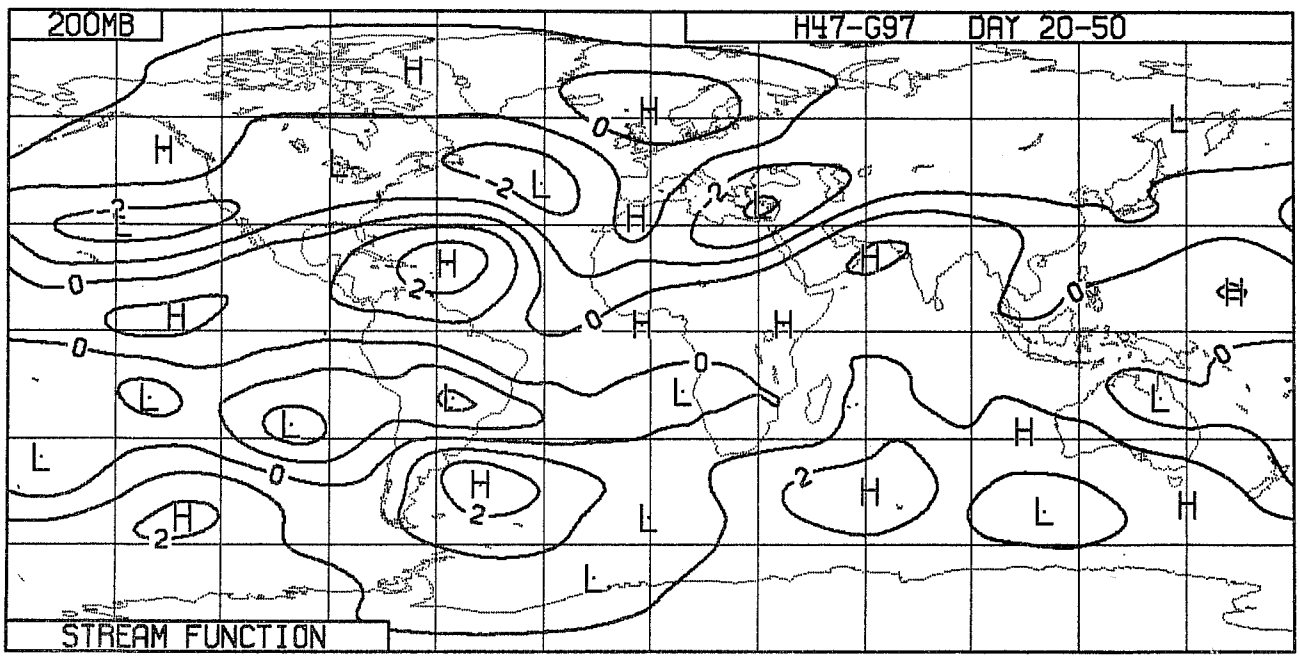

Fig. 24 Differences of 30 day mean 200 mb stream function between the two simulations (A-S minus Kuo).

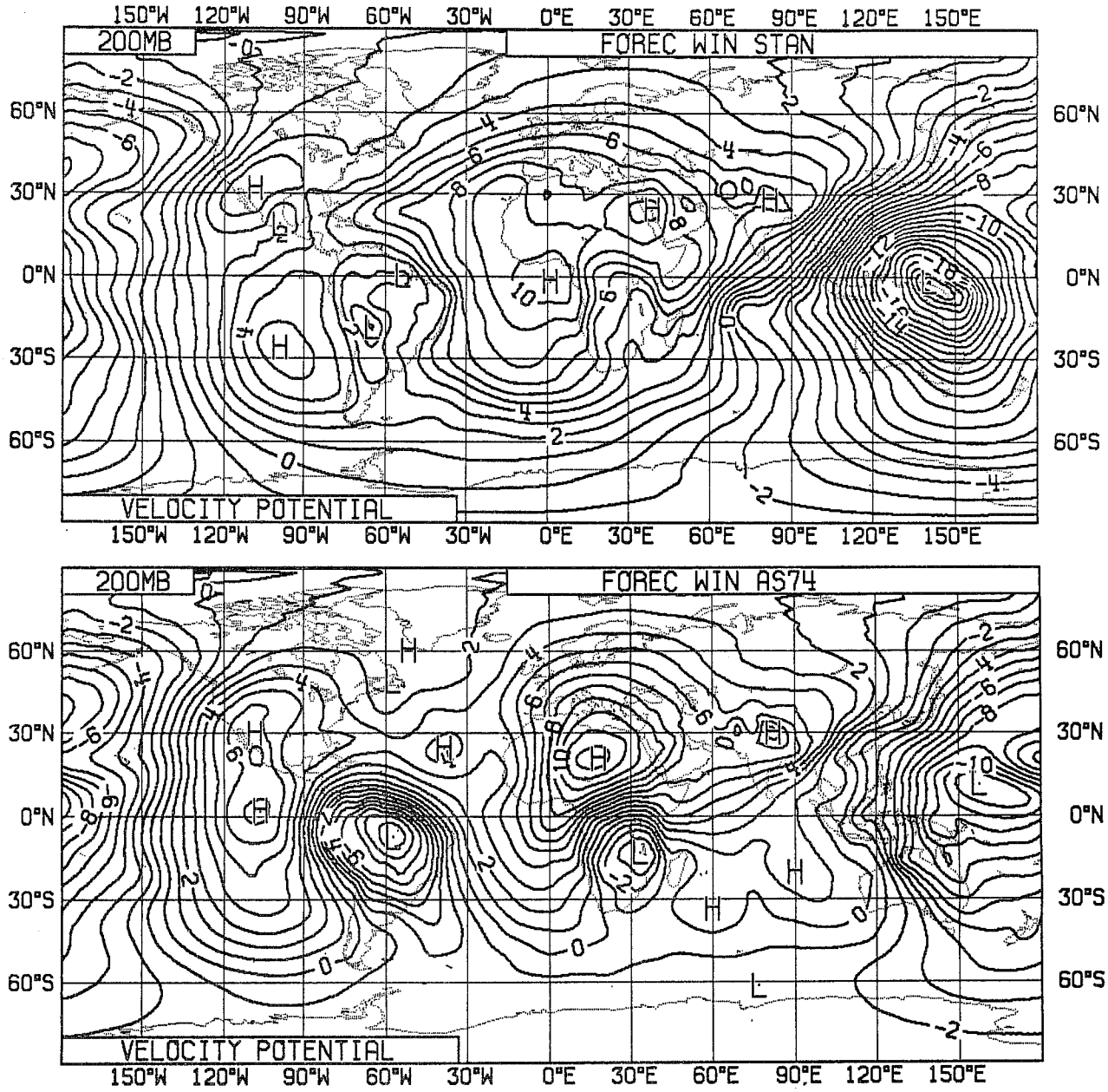

Fig. 25 Simulated 30 day mean velocity potential at 200 mb for simulations with Kuo-scheme (top) and with A-S scheme (bottom).

In the tropics and subtropics the differences are predominant in the divergent component of the mean flow. From the mean velocity potential distribution at 200 mb (Fig.25) it can be seen that the simulation with the A-S scheme favours a strong diffluent flow over South America and South Africa whereas the divergent flow over the western Pacific and Indonesia is much weaker than in the control run. As the tropical divergent flow is presently not well analysed (in particular not the monthly mean flow and its interannual variability) it is difficult to judge how realistic the simulated flow is. There are, however, indications that the diabatic forcing is unrealistic in the simulation with the A-S scheme. Comparing the precipitation rates obtained in the simulations (Fig.26) with the climate values given by Jäeger for February (Fig.18a) we find excessive precipitation rates in the simulation with the A-S scheme over South America and Africa. This excessive precipitation over the tropical continents is related to the lack of clouds used for the radiation calculation in those areas. Although the cloud-cover is calculated in the same way in both integrations, i.e. from the grid-sccale relative hummidity field, the cloud cover in the tropics is considerably smaller in the simulation with the A-S scheme than in the control experiment. As a result of the reduced cloud cover more solar radiative energy is absorbed at the surface (Fig.27) being available for evapotranspiration which in turn drives moist convection. The deficiency in the convective cloud cover parameterized in connection with the A-S scheme may be explained by the inherent tendency of the A-S scheme to systematically dry out the atmosphere which necessarily leads to smaller cloud amounts derived from the relative humidity field.

In summary we may conclude from this experiment:

(I) The simulated mean tropical and extratropical flow are found to be sensitive to the parameterization of convection.

(II) No conclusive evidence is found as to which convection scheme (Kuo or A-S) is more suitable for a GCM.

(III) This experiment suggests that convection cannot be treated in isolation but must include the cloud-radiation feedback.

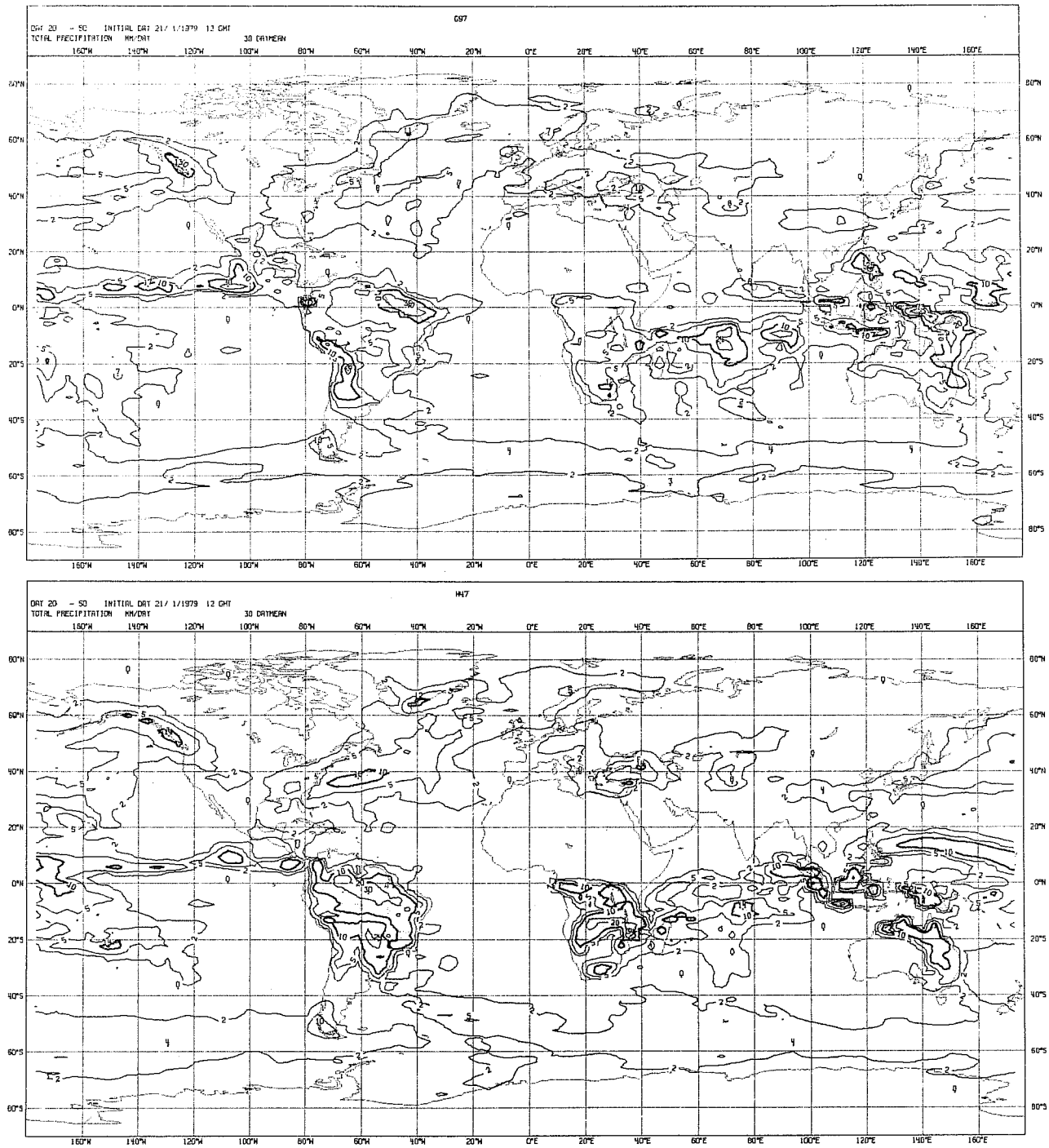

Fig. 26 30 day mean precipitation rate for simulations with Kuo-scheme (top) and with A-S scheme (bottom).

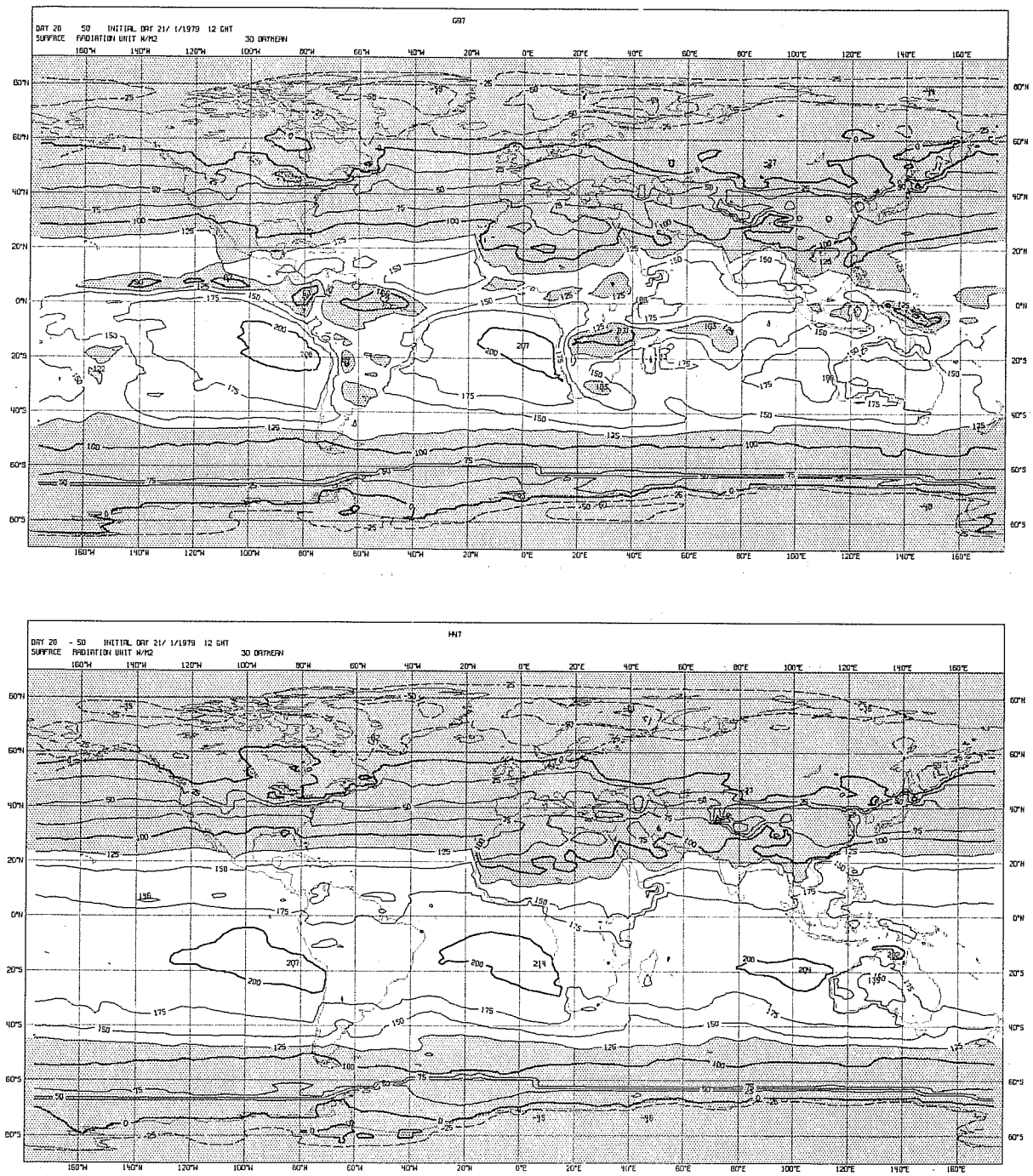

Fig. 27 30 day mean surface radiation flux for simulations with Kuo-scheme (top) and with A-S scheme (bottom). Values below 125 W/m^2 are stippled.

REFERENCES

Arakawa, A. and W.H. Schubert, 1974: Interaction of a cumulus cloud ensemble with the large-scale environment. J.Atm.Sci., 31, 674-701.

Baumgartner, A., 1981: Water Balance. In JSC Study Conferene on "Land surface processes in atmospheric general circulation models", Greenbelt, USA, 5-10 January 1981, pp.515-540.

Burridge, D.M. and Haseler, J., 1977: A model for medium range weather forecasts - adiabatic formulation. ECMWF Tech.Rep.No.4.

Clapp, P.F., 1961: Normal heat sources and sinks in the lower troposphere in winter, Mon.Wea.Rev., 89, 147-162.

Crutcher, H.L. and Jenne, R.J., 1970: An interim note on Northern Hemispheric climatological grid data tape NOAA. Environment Data Service, NWR, Ashevile.

Dopplick, T.G., 1972: Radiative heating of the global atmosphere. J.Atmos.Sci., 29, 1278-1294.

Dopplick, T.G., 1979 Corrigendum. J.Atmos.Sci., 36, 1812-1817.

Erbensen, S.K. and Kushnir, Y., 1981: The heat budget of the global ocean. An atlas based on estimates from surface marine observations. Climatic Research Institute, Report No.29, Oregon State University, Corvallis, Oregon.

Han, Y-J. and Le, S-W., 1981: A new analysis of monthly mean wind stress over the global occean. Climatic Research Institute, Report No.26, Oregon State University, Corvallis, Oregon.

Jaeger, L., 1976: Monatskarten des Niederschlages für die ganze Erde. Ber.Dtsch.Wetterd., Offenbac/Main, No.139, Vol.18, 38pp.

Manello, L.P., 1979: Earth Atmosphere Radiation budget derived from NOAA satellite data June 1974-February 1979. NOAA S/T 79-187, Vol.1 and 2.

Oort, A.H., 1964: On estimates of the atmospheric energy cycle. Mon.Wea.Rev., 92, 483-493.

Oort, A.H. and Rasmussen, E.M., 1971: Atmospheric circulation statistics, NOAA Professional Papr 5, pp.323

Schutz, C. and Gates, W.L., 1971: Global climatic data for surface, 800 mb, 400 mb: January. The Rand Corp, R-915-ARPA

Schutz, C. and Gates, W.L., 1972: Global climatic data for surface, 800 mb, 400 mb: July. The Rand Corp, R-1029-ARPA.

Tiedtke, M., J-F. Geleyn, A.Hollingsworth, J-F.Louis, 1979: ECMWF model, parameterization of subgrid scale processes. ECMWF Tech.Rep.No.10.